Projected future changes in extreme precipitation over China under stratospheric aerosol intervention in the UKESM1 climate model

Ou Wang[1], Ju Liang[2], Yuchen Gu[3], Jim M. Haywood[4,5*], Ying Chen[6], Chenwei Fang[7], Qin`geng Wang[1*]

[1]State Key Laboratory of Pollution Control and Resources Reuse, School of Environment, Nanjing University, Nanjing, 210023, China
[2] Department of Agricultural Meteorology, College of Resources and Environmental Sciences, China Agriculture University, Beijing 100193, China
[3]Department of Earth Science, Mathematical and Physical Sciences, University College London, London WC1E 6BT, UK
[4]Department of Mathematics, Faculty of Environment, Science and the Economy, University of Exeter, Exeter EX4 4QE, UK
[5]Met Office Hadley Centre, Exeter EX1 3PB, UK
[6]School of Geography Earth and Environment Sciences, University of Birmingham, Birmingham B15 2TT, UK
[7]Key Laboratory of Meteorological Disaster, Ministry of Education (KLME), Joint International Research Laboratory of Climate and Environment Change (ILCEC), Collaborative Innovation Centre on Forecast and Evaluation of Meteorological Disasters, Key Laboratory for Aerosol-Cloud-Precipitation of China Meteorological Administration, Nanjing University of Information Science & Technology, Nanjing, 210044, China

Correspondence to: Qin`geng Wang (wangqg@nju.edu.cn), Jim M. Haywood (J.M.Haywood@exeter.ac.uk)

Abstract. Extreme precipitation events are linked to severe economic losses and casualties in China every year; hence, exploring the potential mitigation strategies to minimize these events and their changes in frequency and intensity under global warming is of importance, particularly for the populous subregions. In addition to global warming scenarios, this study examines the effects of the potential deployment of stratospheric aerosol injection (SAI) on hydrological extremes in China based on the SAI simulations (G6sulfur) of the Geoengineering Model Intercomparison Project (GeoMIP) by the UK Earth System Model (UKESM1) simulations. The G6sulfuris compared with simulations of the future climate under two different emission scenarios (SSP5-8.5 and SSP2-4.5) and reduction in the solar constant (G6solar) to understand the effect of SAI on extreme precipitation patterns. The results show that, under future simulations (SSP5-8.5 and SSP2-4.5), precipitation and extreme wet climate events during 2071-2100 are projected to increase relative to the control period (1981-2010) across all the subregions in China. Extreme drought events show a projected increase in southern China. The G6sulfur and G6solar experiments ameliorate the increases in extreme rainfall intensities, especially for the eastern subregions of China. The efficacy of SAI in decreasing extreme precipitation events and consecutive wet days are more pronounced than that of G6solar. While the G6sulfur and G6solar show encouraging potential abatement of the impacts from detrimental extreme events which are similar with the lower emissions target of SSP2-4.5, there are some exceptions. For instance, both G6sulfur and G6solar show drying at high latitudes regions, which is consistent with our understanding of the spin-down of the hydrological cycle under

SRM. These side effects imply that a cautionary approach and further optimization may be required should any future SRM deployment be considered.

1 Introduction

China, as a country that hosts the world's second largest population, is acutely vulnerable to extreme hydrological events caused by climate change. For example, climate change can cause sea-level rise which could significantly impact flooding hazards for coastal cities in China, and flooding events in China are consistently projected to increase under the influence of rising greenhouse gas (GHG) emissions. For example, studies show that precipitation and flooding caused by heavy rainfall events will increase across China by the end of the 21st century (Ying et al., 2014; Yang et al., 2021; Zhnag and Zhou,, 2020). Extreme precipitation events appear to have impacted China more often in recent years. For example, in the summer of 2020,with severe flooding occurred in southern, eastern, and parts of central China (Jia et al., 2022). In the summer of 2021, unprecedented rainfall hit Zhengzhou, with an intensity of over 200 mm per hour (Zhao et al., 2021) and over 550 mm within 24 hours (Dong et al., 2022). In 2022, although southern China continued to suffer from extreme precipitation, the flooding was centring in the west of the Yangtze River, including provinces such as Sichuan and Qinghai which have experienced sudden heavy rainfall events. In July of 2023, a record-breaking episode of rainfall and flooding unfolded across at least 16 cities and provinces in north-eastern China. Notably, Beijing encountered the most substantial precipitation event in the past 140 years, with accumulated rainfall exceeding 60% of the region's typical annual precipitation within a remarkably brief span of 83 hours (CDP, 2023). Although not statistically robust, these events might tentatively suggest a potential expansion of regions that could be influenced by increasing precipitation under the changing climate. On a global scale, climate change has been influencing hydroclimatic conditions (Donat et al., 2016; Pendergrass and Knutti, 2018). The direct influence of global warming is that rising atmospheric temperatures induce stronger evapotranspiration and the atmosphere can hold more water vapour. The intensified hydrological cycle exacerbates heavy rainfall and flooding but can also contribute to further drying over land areas and prolonged drought periods (IPCC, 2021). Consequently, Precipitation tends to increase significantly during events commonly classified as extreme in response to warming (Pendergrass and Knutti, 2018). Extreme weather events including droughts and flooding could be worsened by global warming. A global-scale study indicates that global warming will potentially increase drought severity as well as drought frequency in the future (Qi et al., 2022). Flooding events also occur at higher frequency and intensity under extreme precipitation amplification (Tabari, 2020). Weather and climate disasters such as extreme temperatures and severe snowstorms, have caused serious economic losses in densely populated East Asian countries (Huang et al., 2007; Li et al., 2016). An increase in precipitation forecasted by current climate models, particularly over the populated areas in East Asia, such as China (Liang and Haywood., 2023) implies strategies are urgently needed to mitigate changes in hydrological extremes.

Owing to the difficulties in achieving climate targets such as the 1.5°C or 2°C above pre-industrial levels proposed by the Paris Conference of Parties (IPCC, 2018), Solar Radiation Modification (SRM) proposals, i.e. strategies to mitigate the worst impacts of climate change by brightening the planet have been studied (Haywood et al., 2022). To understand the robust climate model responses to geoengineering, the Geoengineering Model Intercomparison Project (GeoMIP) was established to provide a comprehensive multi-model assessment of the effects of SRM (Kravitz et al., 2013; Kravitz et al., 2011). G6sulfur experiment is one of the most prominent SRM strategies of recent simulations (Visioni et al., 2022). To some extent, SAI can partially counteract climate warming by injecting reflective particles, or their gaseous precursors, into the stratosphere (Zarnetske et al., 2021). In addition to reducing the temperature, SAI also influences tropospheric and stratospheric ozone, terrestrial ecosystem, terrestrial carbon, and hydrological cycle by changing the physical climate system and atmospheric chemistry. Numerous studies support these effects associated with volcanic eruptions and their simulation through SAI techniques (e.g. Imai et al., 2020; Mclandress et al., 2011; Jones et al., 2018, 2020; Liang and Haywood., 2023; Lee et al., 2021; Plazzotta et al., 2019; Visioni et al., 2022).The latest phase of policy-relevant GeoMIP simulations (GeoMIP6) proposed two new experiments, G6sulfur and G6solar (Kravitz et al., 2015), which are designed to simulate the influence of SAI and solar constant reduction to the end of the 21st century based on predicted future emission pathways (Shared Socioeconomic Pathway; SSPs). G6sulfur and G6solar aim to lower global mean surface temperatures from a high-tier emission scenario (SSP5-8.5; Meinshausen et al., 2020) to a medium-tier emission scenario (SSP2-4.5). These SSP scenarios were developed by the Coupled Model Intercomparison Project Phase 6 (CMIP6; Eyring et al., 2016), which provides multi-model climate projections based on alternative scenarios of future emissions and land use changes produced by integrated assessment models (O'neill et al., 2016). Studies such as Jones et al. (2021) and Ji et al. (2018) included detailed descriptions and explanations of the CMIP6, GeoMIP, and the differences in models' assumptions. Previous studies indicated SAI would exert a negative radiative forcing and reduce near-surface air temperature (including temperature means and extremes), and precipitation (Pinto et al., 2020; Liu et al., 2021). For example, The GLENS experiments revealed significant alterations in precipitation patterns across tropical and midlatitude regions when sulfate geoengineering counteracts global warming (Simpson et al., 2019). However, as suggested by some studies, although SAI can effectively counteract anthropogenic global warming at the global scale, it cannot fully offset the effects at regional scale (Niemeier et al., 2013; Tilmes et al., 2013; Tye et al., 2022). Furthermore, the climate effects in terms of magnitude as well as spatial and temporal distribution depend largely on the scenario of SAI deployment. To date, only a few studies have concentrated on the impact of SAI on the future changes in weather systems over East Asia (Liang and Haywood., 2023; Liu et al., 2023; Tew et al., 2023).

In this study, we focus on the potential effects of SAI geoengineering on hydrological extremes over China. Based on simulations of the UKESM1 model and CMIP6 experiments, our study explores the changes in frequency and intensity of extreme precipitation between the latest future GHG emission scenarios and solar geoengineering (G6sulfur, G6solar). The results of the period towards the end of this century, 2070-2100, were compared with that of control period (CP: 1981-2010). Section 2 describes the experimental design and details of the model used in this study. In Section 3, results are presented to

show the changes in extreme indices in China under the SAI (G6sulfur) and solar constant reduction (G6solar) during 2071-2011, compared to control period and future emission scenarios (SSP5-8.5, SSP2-4.5). The regional analysis of China's extreme precipitation and cumulative distribution function is also provided in Section 3. Section 4 summarises and discusses the findings.

2. Data and methods

2.1 Study area

To quantitatively examine regional differences and better visualize the future extreme climate features, China is divided into 7 different sub-regions (Fig.1) to distinguish extreme climates across the following regions: Northeast China (NEC), North China (NC), Northwest China (NWC), Centre China (CC), East China (EC), South China (SC), and Southwest China (SWC) following Liang et al. (2023).

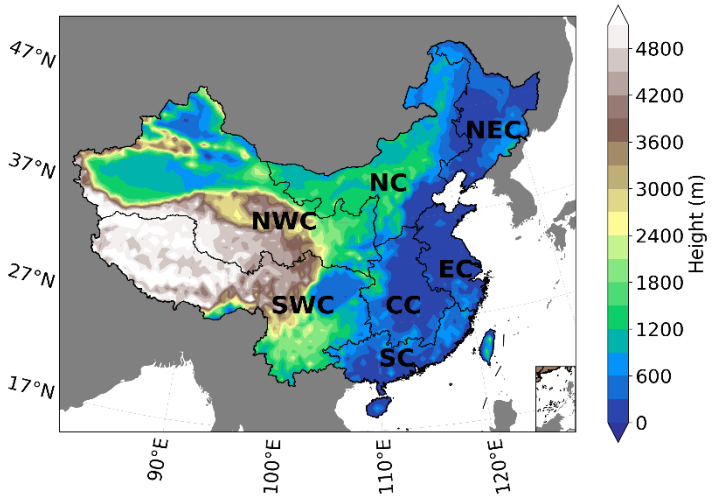

Figure 1: Geological map of elevation and 7 sub-regions in China (unit: m), data from (Liang et al., 2023)

2.2 UKSEM1 model and model simulations

This study was based on the simulations by the U.K. Earth System Model UKESM1 (Sellar et al., 2019). UKESM1 contains the sophisticated United Kingdom Chemistry and Aerosols (UKCA) module that represents the sulphur cycle in the troposphere and stratosphere (Archibald et al., 2020), is a fully coupled model with a resolution of 1.25° latitude by 1.875° longitude (Storkey et al., 2018; Walters et al., 2019; Mulcahy et al., 2018, Sellar et al., 2019), and contributes to both CMIP6 and GeoMIP6 (Jones et al., 2020). The Scenario MIP high GHG forcing scenario SSP5-8.5 (O'neill et al., 2016) is used as the

baseline scenario of both G6solar and G6sulfur experiments (Kravitz et al., 2015). In the G6sulfur experiment, UKESM1 simulates SO_2 injection in the stratosphere along the Greenwich meridian at an altitude of 18-20 km between 10° N and 10° S (Kravitz et al., 2021; Haywood et al., 2022). A parallel experiment to the G6sulfur, the G6solar experiment, reduces ScenarioMIP Tier 1 high forcing scenario to the medium forcing scenario by reducing solar irradiance. Notably, it is anticipated that the G6solar will exhibit reduced inter-model disparities in the spatial distribution of forcing when compared to the G6sulfur owing to model differences in representing the complexities of the sulfur cycle within global models. Therefore, the G6solar is proposed as a parallel experiment to the G6sulfur for the purpose of comparing the impacts of solar reduction with those of stratospheric aerosols. (Kravitz et al., 2015).

In the UKESM1 model, three ensemble members, 'r1i1p1f2', 'r4i1p1f2', and 'r8i1p1f2', are run for the G6sulfur and the G6solar as specified in the GeoMIP protocol (Kravitz et al., 2015). We calculated the ensemble mean for all simulations, including SSP5-8.5, SSP2-4.5, G6sulfur, G6solar and Historical. The future changes in extreme climates were assessed by comparing the future simulations (SSP5-8.5, SSP2-4.5, G6sulfur, G6solar) for the period 2071-2100 with the control period 1981-2010, using the UKESM1 historical simulations for CMIP6. The results for the future 30 years of the 21st century (2071-2100) from the simulations were used to investigate the influences of the G6sulfur and the G6solar experiments.

2.3 Aphrodite precipitation data

The APHRODITE (Asian Precipitation-Highly-Resolved Observational Data Integration Towards Evaluation) was interpolated from gauge-observation data with a resolution of 0.25°× 0.25° (Lai et al., 2020; Yatagai et al., 2012), and were used to validate the performance of the UKESM1 model in simulating the control period extremes. APHRODITE has been a dataset containing long-term gridded daily precipitation (1951-2015). The high-resolution daily product of APHRODITE is developed based on the rain-gauge data across Asia presented on a continental scale (Sunilkumar et al., 2019). In this study, we applied the APHRODITE's climatological daily mean precipitation as observation data for validating the UKEMS1 simulations.

2.4 Extremes precipitation indices

To quantify extreme precipitation, a range of indices were defined by the World Climate Research Programme (WCRP). In this study, eight extreme indices were selected according to the WCRP's Expert Team on Climate Change Detection and Indices (ETCCDI), as shown in Table 1.

Table 1: The definition of selected extreme indices based on ETCCDI (Firch et al, 2002; Klein Tank et al., 2009)

Indices	Descriptive name	Definition	Units
DD	Dry days	Count of days when precipitation<1 mm	days
CDD	Consecutive dry days	Maximum number of consecutive days with < 1 mm of precipitation	days
CWD	Consecutive wet days	Maximum number of consecutive days with ≥ 1 mm of precipitation	days
R50MM	Rainstorm days	Count of days when precipitation≥50 mm	days
RX1DAY	Maximum 1-day precipitation	Annual maximum 1-day precipitation	mm
RX5DAY	Maximum 5-day precipitation	Annual maximum consecutive 5-day precipitation	mm
R95p	Very wet days	Annual precipitation amount accumulated on days when daily precipitation is greater than the 95th percentile threshold of the wet-day precipitation	mm

2.5 Statistical methods and Cumulative Distribution Functions (CDFs)

At first, for validating the model simulations, the Aphrodite data was re-gridded to the resolution of the UKESM1 ensemble mean data. To examine the statistical importance of the changes in precipitation between different experiments, we performed the Wilcoxon Rank Sum Test. Wilcoxon Rank Sum Tests works as a non-parametric two-sample t-test and is more appropriate for use with atmospheric data (Wilks, 2011), with a 5% confidence level of statistical significance.

To better visualize the future extreme climate features and the effects of SAI, the Cumulative Distribution Functions (CDFs) for rainfall have been calculated. CDFs is frequently employed for bias correction to enhance the accuracy of rainfall analysis (e.g., Apurv et al., 2015; Rana et al., 2014; Xiong et al., 2019). This approach allows for a nuanced exploration of the distribution, accommodating the continuous and discrete aspects of our dataset. The calculated CDFs offer a holistic perspective, providing insights into the probability distribution patterns for various events over the study period.

Unlike Tung et al. (2022), where CDFs were employed, a choice was made to use reversed CDFs in our study to better illustrate the thresholds for rainfall events exceeding certain values. To achieve this, during the continuous 30-year study period, we

computed the average annual extreme precipitation index values for each grid point and plotted their CDFs over all grid points in a region. This analysis facilitated the observation of continuous probability distribution patterns and the assessment of tail-end magnitudes, providing insights into the continuous likelihood of varying precipitation levels and revealing extremes throughout the studied period.

3. Results

3.1. Precipitation changes

Figure 2 shows spatial distribution of observed and simulated mean precipitation over China during the control period (CP; 1981-2010) and comparisons between the two datasets. While the general pattern of the simulated precipitation (Fig.2b) was similar to the observed precipitation (Fig.2a), the amount of precipitation simulated tends to be somewhat larger than the observed over much of China, as indicated in Fig.2c. Both results show a general decreasing trend from the southeast coastal regions to the northwest inland areas. The wet bias in daily precipitation is evident in most parts of southern China (SC, CC, and SWC), particularly on the south-eastern flanks of the Qinghai-Tibet Plateau (QTP). Regions with dry bias are relatively small (shown by the negative values and brown contours in Fig.2c), with bias values less than 1 mm day^{-1}.

To further compare the results between simulations and observations, particularly focusing on extreme precipitation values, a scatter plot between the ensemble mean simulations and observations is provided as Fig.2d (the scatter plots comparing the simulations of the three model ensembles with the observations are provided in Fig.S1). For the purpose to evaluate the model performance at different level of precipitation, the daily precipitation was as classified in to several intervals: P10 (the smallest 10%), P10-50, P50-90, P90-95, and P95 (the largest 5%). In order to indicate the bias as a percent, relative changes (compared to the observations) for different intervals have been calculated, as listed in Table 2.

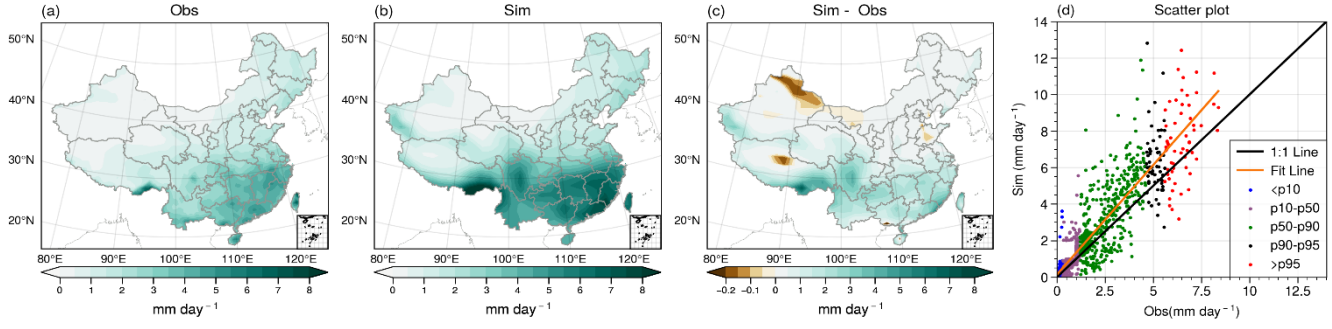

Figure 2. Spatial distributions of mean land precipitation (units: mm day^{-1}) over China during the control period of 1981-2010 for (a) the observations (Obs), (b) the simulations (Sim), (c) the bias (Sim-Obs), and (d) a scatter plot between the observations and simulations at different level of precipitation.

Table 2: Relative changes of the model results (compared to the observations)

intervals	Ensemble mean	r1i1p1f2	r4 i1p1f2	r8i1p1f2
<P10	89.81%	93.95%	89.44%	86.04%
P10-50	30.05%	30.38%	31.85%	27.13%
P50-90	30.50%	28.95%	31.36%	31.16%
P90-95	24.03%	22.79%	24.85%	24.44%
>P95	15.76%	15.09%	16.27%	15.92%

The scatter plots (Fig.2d and Fig.S1) indicate a close relationship between the observations and the simulations. However, the simulations are generally higher than observations, possibly because of the different resolution of the data. Since our study has been mainly focused on the relative changes between the future results and that of control period for different scenarios, the systematic bias would not affect the conclusions significantly. As expected, relative changes are very large at small values (below the 10th percentile), both for the ensemble mean and the model members. For the results at the 10-50th and 50-90th percentiles, relative changes are around 30%. When larger than the 95th percentile, relative changes are relatively small, near 15%. The differences among ensemble members are not significant, which suggests the uncertainty in the ensembled results is reasonable and acceptable.

Figure 3 illustrates the spatial distribution of relative changes in mean precipitation for different simulations during the future period 2071-2100 relative to the control period. In all the four simulations, most part of the region is dominated by increased precipitation. For SSP5-8.5 (Fig.3a), the most prominent increase in precipitation occurs within SC, but the precipitation in SC, northern Taiwan and Hainan is projected to decrease in the future. SSP2-4.5 (Fig.3b), similar pattern can be seen but the magnitude of increases is generally reduced, particularly in SC, by about 50% relative to SSP5-8.5. For G6sulfur (Fig.3c), changes are similar to that of SSP2-4.5, indicating the SAI is approximately successful.

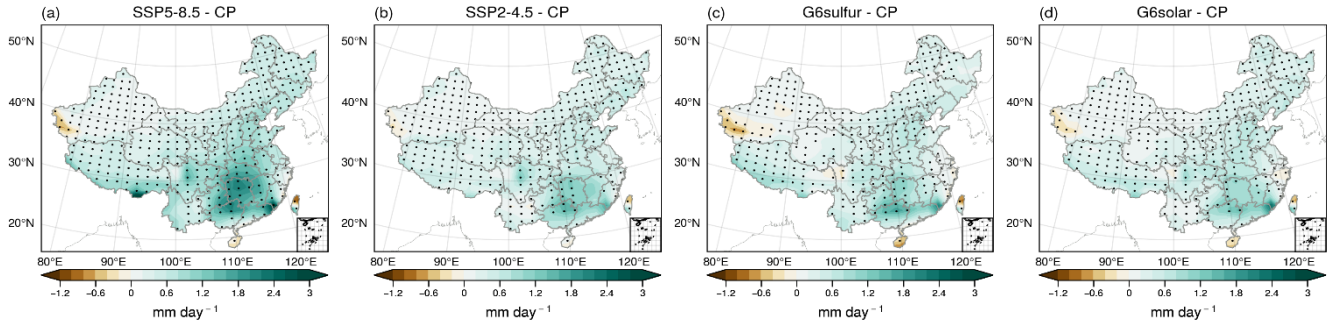

Figure 3. Relative changes in land precipitation (mm day^{-1}) of the period 2071-2100 compared to that of the CP (1981-2010) (a) SSP5-8.5, (b) SSP2-4.5, (c) G6sulfur, and (d) G6solar. The dotted areas indicate where the difference is statistically significant at 95% confidence level using a Wilcoxon rank sum test.

Figure S2 compares the simulated future precipitation between G6sulfur and other experiments. Compared with SSP5-8.5 (Fig. S2(a)), the simulated SAI by G6sulfur leads to a decrease in precipitation over almost the entire China. This suggests that the effect of SAI on future precipitation is more widespread and remarkable compared to that of SSP5-8.5, particularly over the SWC (southeast QTP) and CC regions. The difference in precipitation between G6sulfur and SSP2–4.5 (Fig. S2(b))/G6solar (Fig. S2(c)) is smaller compared to the difference between G6sulfur and SSP5-8.5 (Fig. S2(a)). This indicates SAI effectively mitigates the increase in mean precipitation from the high GHG SSP5-8.5 scenario to the medium GHG SSP2-4.5 scenario across most of China.

3.2. Hydrological extreme changes

3.2.1 Wet extreme changes

The small-scale flooding risk is assessed by the RX1day index, and the extreme threshold index of very wet day precipitation is represented by the R95p,for which the 95th percentile of threshold was computed for each grid based on the 30 years (1981-2010) daily precipitation. The changes in RX1day and R95p for the future period (2071-2100) relative to the control period (1981-2010) are shown in Fig.4. Simulations under the SSP5-8.5 scenario project significant increases (p-value < 0.05) in RX1day in east China (Fig.4a). The greatest magnitude of increase (above 50 mm) is seen in SC, CC, east coastal NC and a small part of SWC regions. Under SSP2-4.5 (Fig.4b), a similar pattern of the RX1day change to SSP5-8.5 is projected but with smaller magnitudes. G6sulfur (Fig.4c) and G6solar (Fig.4d) show generally ameliorated changes compared to SSP5-8.5.

In the future, an increase in RX5day is anticipated across most of China, with the most substantial increments occurring in the eastern part of the country and on the QTP (Fig. S3a-d). The largest increases are anticipated under the SSP2-8.5 scenario

(Fig.S3a), reaching a maximum of over 100 mm. In the other three G6 scenarios, the increase in RX5day is considerably smaller than that under SSP5-8.5, with none exceeding 100 mm compared to the control period (Fig.S3a-d). This suggests a mitigated future RX5day simulation compared to SSP5-8.5 in these three models. It is noteworthy that under G6solar (Fig.S3d), the maximum RX5day is observed in the south-eastern part of the SC region.

R95p is projected to significantly increase in CC, SC, and south SWC regions under SSP5-8.5 scenario (Fig.4e), consistent with a previous study (Wang et al., 2016; Qin and Xie., 2016; Peng et al., 2018). This increase has been attributed to the strengthened south-westerly winds across south China caused by the land-sea contrast between China and adjacent oceans. Furthermore, global warming also contributes to the increased water vapor, thereby enhancing the likelihood of precipitation and related extremes (Tang et al., 2021). The SSP2-4.5, G6sulfur and G6solar experiments present similar spatial distributions, but smaller magnitudes of changes (Fig.4f-h). G6sulfur (Fig.4g) shows a significant decrease in highly populated areas of Hainan (south SC) compared to SSP5-8.5.

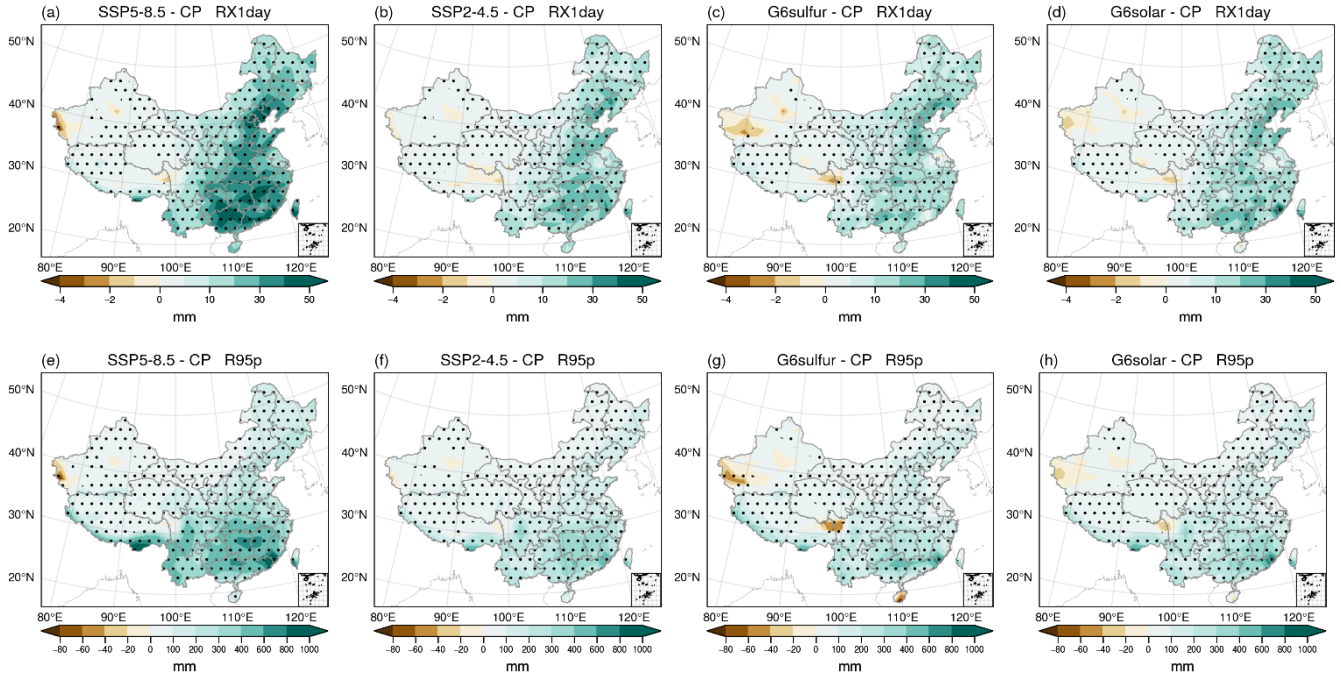

Figure 4. Relative changes in RX1day (a-d) and R95p (e-h) for the future period of 2071 – 2100 compared to the control period (CP). The dotted areas indicate where the difference is statistically significant at 95% confidence level using a Wilcoxon rank sum test.

Figure 5 illustrates how SAI modulates the distribution of extreme precipitation intensity indices by depicting differences between G6sulfur and other experiments. A previous study demonstrated that the reduction of emissions of anthropogenic aerosols is a key factor leading to increased extreme intensity indices over most of China by the end of 21st century (Wang et al., 2016). Compared with SSP2-4.5 (Fig.5b) and G6solar (Fig.5c), G6sulfur leads to only small changes of less than 20mm in RX1day. The similarity of G6sulfur to SSP2-4.5 and G6solar suggests that the primary impact on RX1day over China is driven simply by the temperature; a global mean temperature of the standard CMIP6 SSP2-4.5 scenario gives very similar results to those achieved when SSP5-8.5 temperatures are brought down to those of SSP2-4.5. However, the same cannot be said for R95p, where the ensemble mean of UKESMI projects a significant increase in SC and southwestern SWC (Fig.5e) for the G6sulfur (2071-2100) relative to the SSP2-4.5 (2071-2100), and in north SC, eastern, and southwestern SWC relative to G6solar (Fig.5f).

From Figure S4a, it is evident that G6sulfur effectively mitigates RX5day under SSP5-8.5, particularly in the eastern and south-western regions. The most notable impact is observed in the SC region and the south QTP, with a mitigation of up to 80mm. In comparison to SSP2-4.5 (Fig.S4b), G6sulfur exhibits an increase in RX5day, primarily in the region between 100°E and 120°E. For 'G6sulfur-G6solar' (Fig.S4c), positive values of RX5day are more pronounced in certain areas between 100°E and 120°E, especially in the low latitude zone between 20°N and 30°N.

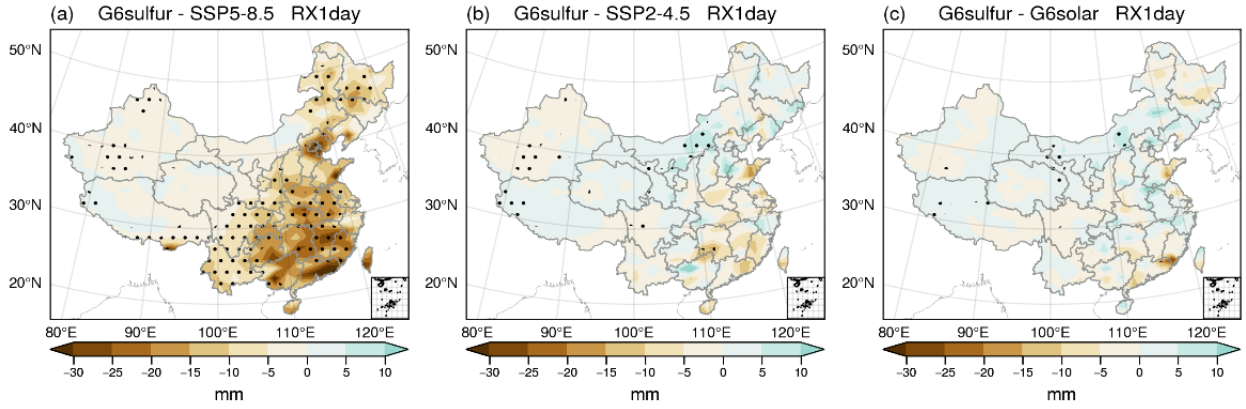

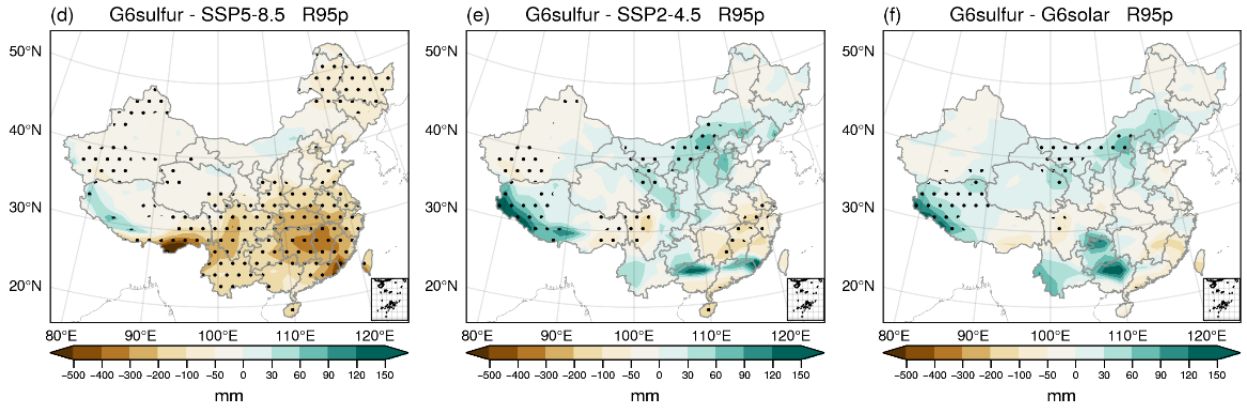

Figure 5. Differences in RX1Day (a-c) and R95p (d-f) for the future period of 2071 – 2100 between G6sulfur and SSP5-8.5 (a, d), SSP2-4.5 (b, e), and G6solar (c, f). The dotted areas indicate where the difference is statistically significant at a 95% confidence level using a Wilcoxon rank sum test.

Table 3 presents the differences in maximum values of the index between the G6sulfur and SSP5-8.5 scenarios. A positive difference suggests a mitigation effect of SAI, while a negative difference indicates exacerbation in index thresholds for projected increase regions. In regions where the projected index is decreasing, the meaning of positive and negative signs is opposite to that in regions where the index is projected to increase. In addition, the 0 values indicate there is almost no difference between the maximum index values under G6sulfur and SSP5-8.5, suggesting negligible impact of SAI on indices threshold. G6solar's ameliorating impact in indices thresholds under the SSP5-8.5 scenario has been presented in Supplement Table S1.

Table 3: Amelioration effect of G6sulfur compared to SSP5-8.5 in indices threshold.

	China	NEC	NC	NWC	EC	CC	SC	SWC
RX1day	+	+	+	+	+	+	+	+
RX5day	+	+	+	+	+	+	+	+
R50mm	+	**0**	+	**0**	+	+	+	+
CWD	-	-	+	+	-	-	-	-
R95p	+	+	+	+	+	+	+	+
DD	-	-	-	-	-	-	+	-
CDD	-	-	-	-	-	-	+	+

RX1day (Fig.6a) and R95p (Fig.6b) show consistent increases in the future relative to control period (the blue line). For RX1day the CDFs for precipitation SSP5-8.5 surpasses those from all other scenarios as might be expected from the spatial analyses presented in Fig.4. Additionally, southeastern China (EC, CC, and SC) shows higher values than the northern and western inland regions (NEC, NC, NWC).

The tail of the RX1day CDFs in experiment G6sulfur (black) is close to that of the SSP2-4.5 scenario (cyan) in NEC, NC, NWC, and SWC (Fig.6). Combined with the small and evenly distributed magnitudes shown in Fig.5b, this shows that G6sulfur effectively mitigates SSP5-8.5 to similar the SSP2-4.5 in these regions. In EC, SC and CC, the RX1day CDFs is reduced from that of SSP2-4.5 by between 5-10mm and moves further away from the values seen in the high-end SSP5-8.5 scenarios towards those seen in the control period simulations. The RX1day CDFs for G6solar are indistinguishable from those for SSP2-4.5 in many regions, but for CC the RX1day lies to the left of the SSP2-4.5 curve but by not as far as that for G6sulfur indicating less abatement of RX1day extremes. Interestingly, for SC, the G6solar CDFs curve lies to the left of the SSP5-8.5 curve. Combining the negative value for the SC region in Table S1 reveals that the maximum value of RX1day under G6solar even further from that of the control period compared to SSP5-8.5, suggesting that while G6solar mitigate the overall RX1day, it exacerbates the maximum RX1day values beyond SSP5-8.5 in the SC region.

The tail of RX5day CDFs across all regions suggests a future increase in RX5day under four G6 scenarios, with a more pronounced rise under the high SSP5-8.5 scenario. This phenomenon is consistent with the spatial distribution change observed in Fig.4(a-d). In the NEC and CC regions, G6sulfur closely aligns with the SSP2-4.5 scenario (Fig. S5). Additionally, in the NC region, G6solar closely mirrors the conditions of the SSP2-4.5 scenario. Combined with the differences in RX5day of spatial distribution in Fig.5, it is evident that G6sulfur mitigates RX5day, resembling the SSP2-4.5 scenario, in NEC and CC regions. Simultaneously, G6solar alleviates RX5day in the NC region, resembling the conditions of the SSP2-4.5 scenario.

For R95p, the CDFs of G6sulfur and SSP2-4.5 show no apparent differences for SC, SWC and NWC; however, in EC and CC, there are decreases of more than 100mm, whereas in NEC and NC, there are some increases about 50mm. For example for the SWC region, Figure 5e reveals that R95p for G6sulfur-SSP2-4.5 shows statistically significant negative values centred at around 30°N 100°E, and statistically significant positive values west of 90°E. Because these regions are aggregated together in the SWC region, there is not a discernible influence on the CDFs of R95p.

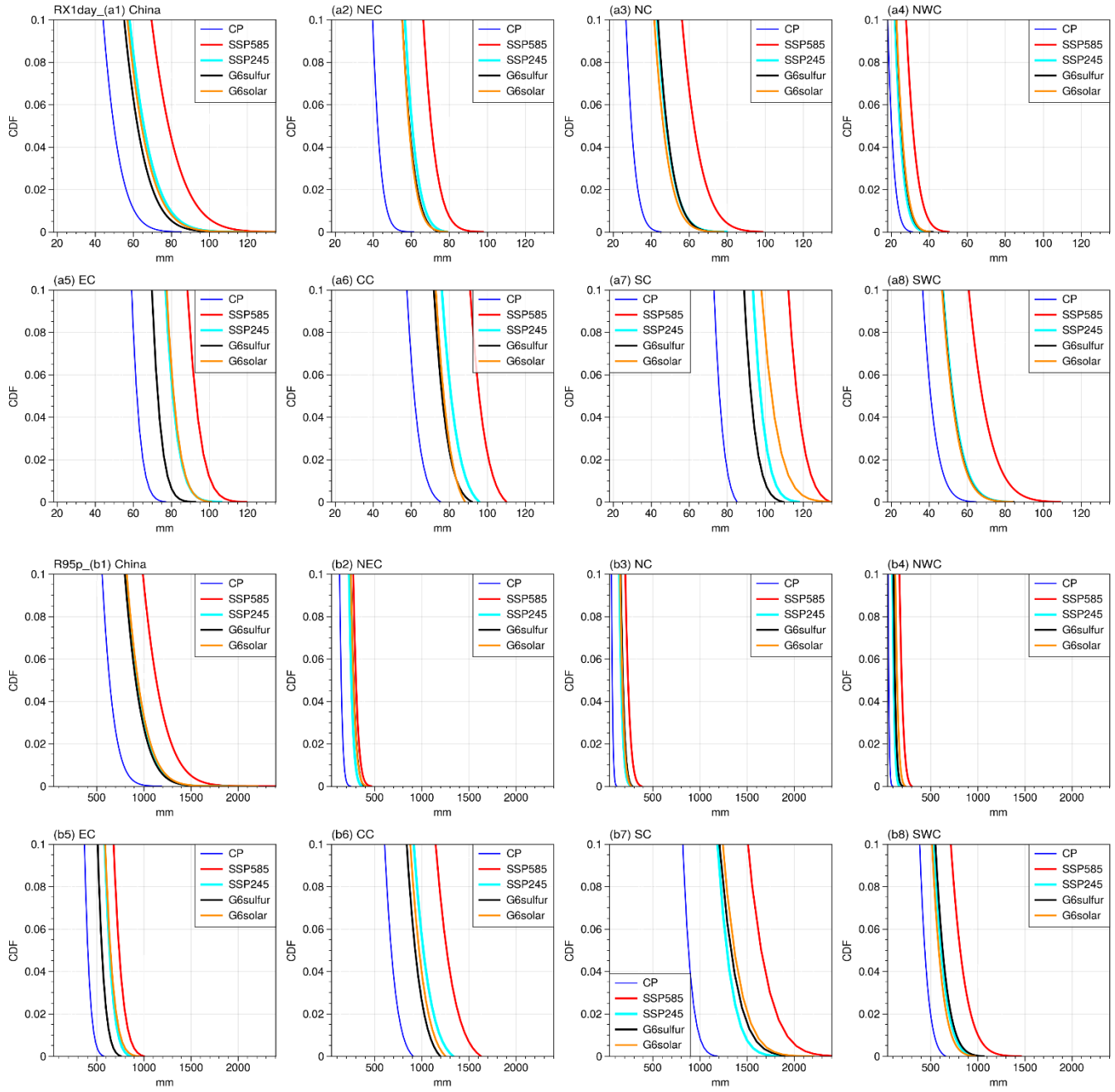

Figure 6. Cumulative distribution functions of RX1day (a1-a8) and R95p (b1-b8) in China and 7 subregions for different scenarios. The same processing was applied to all CDFs figures.

300

In summary, by the late 21st century, eastern China is projected to experience an increase in heavy rain events and a heightened risk of flooding under the high-emission SSP5-8.5 scenario, with UKESM1 simulations indicating a strengthening of both RX1day and R95p, signaling more stronger precipitation events driven by elevated GHG emissions. The SRM results are encouraging, showing a reduction in the detrimental extreme events, similar to the lower emissions target of SSP2-4.5, particularly in east China and QTP region.

The frequency extreme index change in CWD has been calculated and shown in Fig.7. For the SSP5-8.5 scenario (2071-2100) relative to the control period (1981-2010), the ensemble mean of UKESMI predicts a significant decrease in southwest China (Fig.7a), particularly in the south SWC (QTP), with up to 30-day reduction. This reduction could be influenced by the East Asian and South Asian monsoons under the complex terrain of QTP (Wang et al., 2018). The daily extreme precipitation intensity may rise in southern areas China in the future (Zhu et al., 2018). The increased CWD occurs in mid-latitudes (mostly north of 30°N latitudes) but with a lesser extent (less than 20 days). A similar pattern of change is seen under SSP2-4.5, but with smaller magnitudes (Fig.7b). The experiments G6sulfur (Fig.7c) and G6solar (Fig.7d) exhibit generally mitigated changes compared to SSP5-8.5, although the brown areas shown in Fig.7c are larger than in Fig.7a in NWC.

The R50mm index is derived from the Rnnmm index, as suggested by ETCCDI. The Rnnmm index represents the count of precipitation above a user-chosen threshold. In this case, the threshold is set to 50 mm, as recommended by the China Meteorological Administration (CMA) (Sui et al., 2018). Under the SSP5-8.5 scenario (2071-2100) relative to the control period (1981-2010), the ensemble mean of UKESMI projects a significant increase in populous southern and eastern China (Fig.7e). This aligns with a prior study by Meng et al. (2021), which predicts an increase in R50mm in the lower reaches of the Yangtze River basin and the coastal areas in SC (Meng et al., 2021), indicating a rise in rainstorm events in these regions by the end of the 21st century. This increase in rainstorm events contributes to an elevation in precipitation levels (as shown in Fig.3), exerting significant pressure on social economies and terrestrial ecosystems (as discussed by Peng et al., 2018). A similar pattern of change is observed under SSP2-4.5 (Fig.8f) and in the experiments G6sulfur (Fig.8g) and G6solar (Fig.8h), albeit with smaller magnitudes.

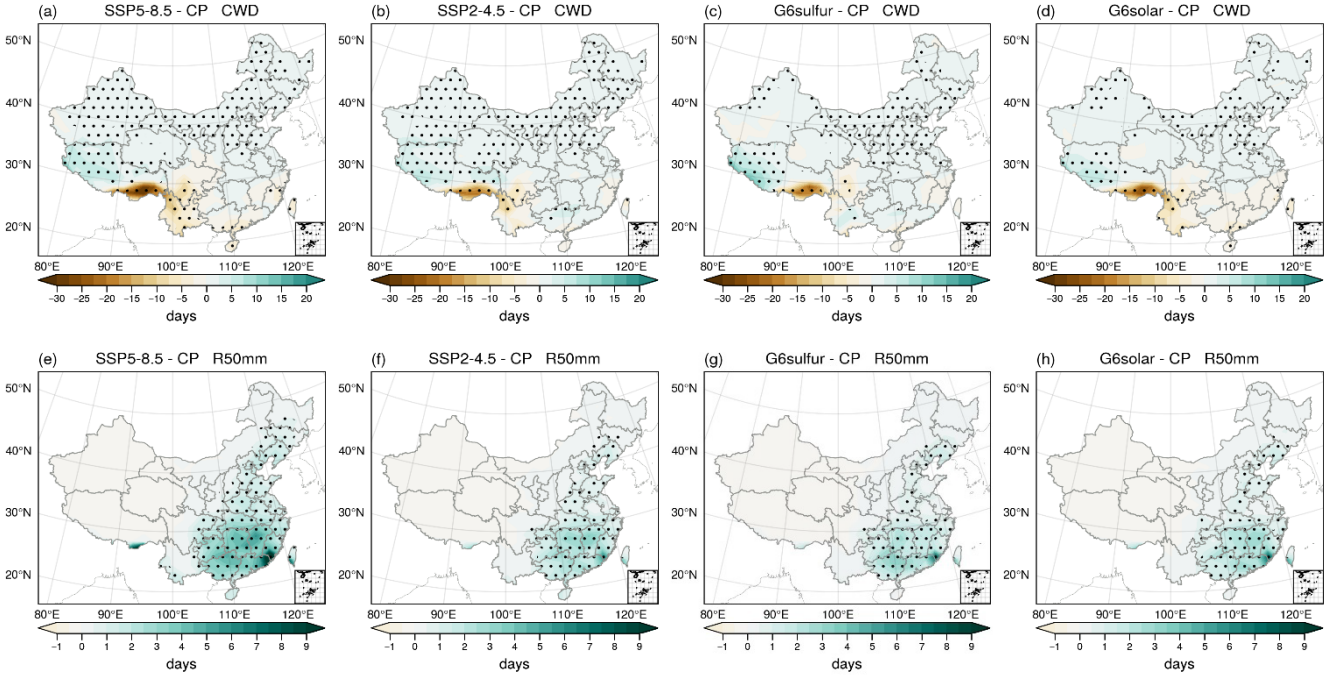

Figure 7. Same as Figure 4, but for CWD (a-d) and R50mm (e-h).

Compared to SSP5-8.5 (Fig.8a), G6sulfur significantly increases the CWD in south SWC (by up to 12 days), indicating sensitivity to globe warming within this region. Combined with Fig.7, G6sulfur decrease in CWD under SSP5-8.5 in southeast QTP (approximately 90°E - 100°E). However, in southwest QTP and south China, G6sulfur exacerbates the increase in CWD compared to SSP5-8.5, possibly linked to the weakening of the high-altitude westerly jet (driven by the reduced meridional thermal gradient under SAI) that induce an anomalous cyclonic flow dominating QTP (Liang and Haywood, 2023) as per the four-quadrant strait jet model (Uccellini and Johnson, 1979), which creates a precipitation-favouring environments. G6sulfur primarily ameliorates the increase in CWD in mid-latitudes (north of 30°N). G6solar (Fig.8c) shows a similar magnitude in south CC and north SC as Fig.8a, suggesting that solar constant reduction does not have a significant effect in CWD compared to SSP5-8.5. For rainstorm (R50mm), G6sulfur leads to a decrease in most part of China, with a significant decrease in south-eastern coastal areas and south QTP, up to 6 days compared to SSP5-8.5. Compared to SSP2-4.5 and G6solar, the differences are close to zero, suggesting that SRM yields nearly identical results to the SSP2-4.5 scenario.

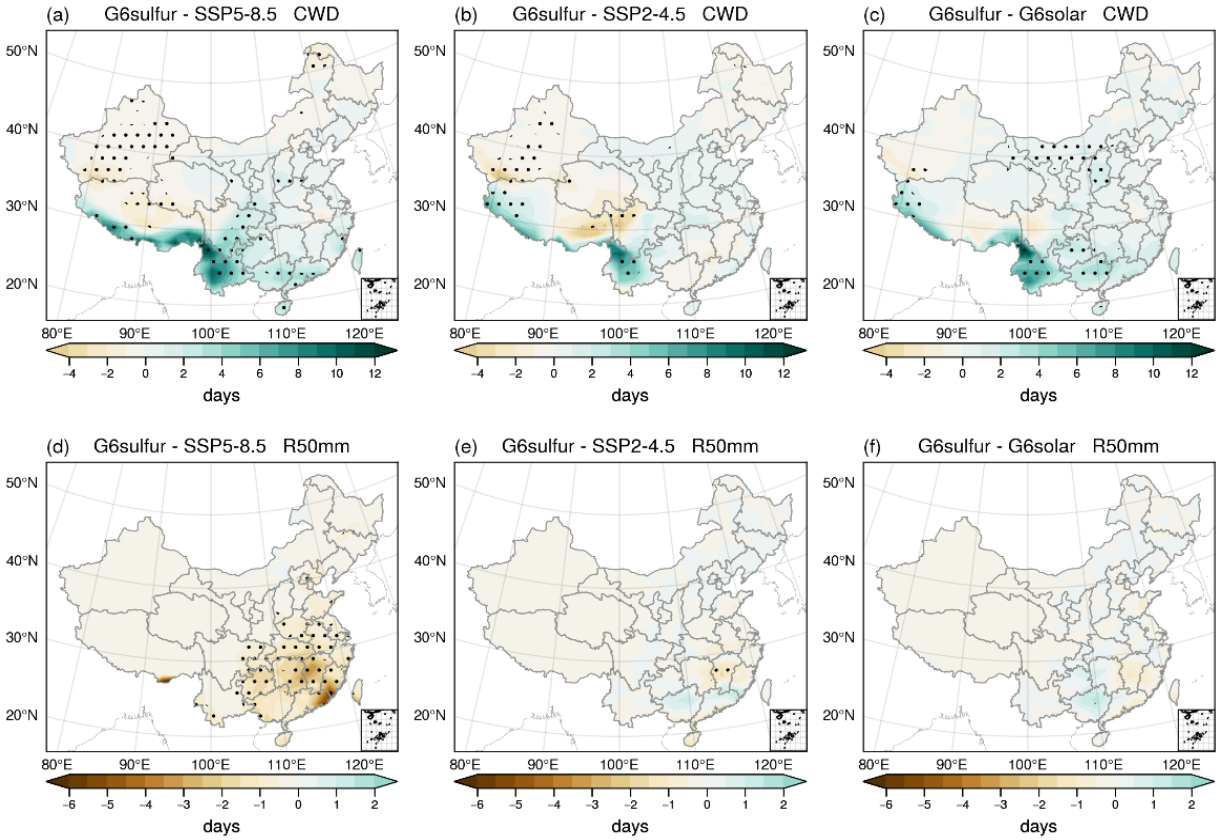

Figure 8. Same as Figure 5, but for CWD (a-c) and R50mm (d-f).

345 The maximum value of CWD in SWC exceeds 200 days, as shown in Fig.9, contributing to a general increase across China (Fig9(a1)). Meanwhile, CWD are projected to decrease, especially in SWC in Fig.9(a8)) and corresponds to the brown shaded areas in SWC as depicted in Fig.7(a-d). In the regions projected to experience an increase of CWD in NE and NWC, the positive value (in Table 3) indicates that SAI experiments produce results of threshold that are closer to the CP conditions. However, the relative effect is not obvious due to the small magnitude of CWD in these regions. It is notable that in NC and
350 SC, G6sulfur (black) provides similar results to the SSP2-4.5. Interestingly, for EC, SSP2-4.5 yields almost identical statistics to SSP5-8.5, while both G6sulfur and G6solar show an increase compared to SSP scenarios. 3 Figure 8(d-f) highlights subtle differences between SSP2-4.5 and SRM strategies. Considering the small magnitude of projected changes and the relatively minor differences in changes between G6sulfur and the other three simulations, coupled with the statistical significance observed in only a few areas in the eastern part. discussions regarding the CDFs of R50mm will be omitted.

355

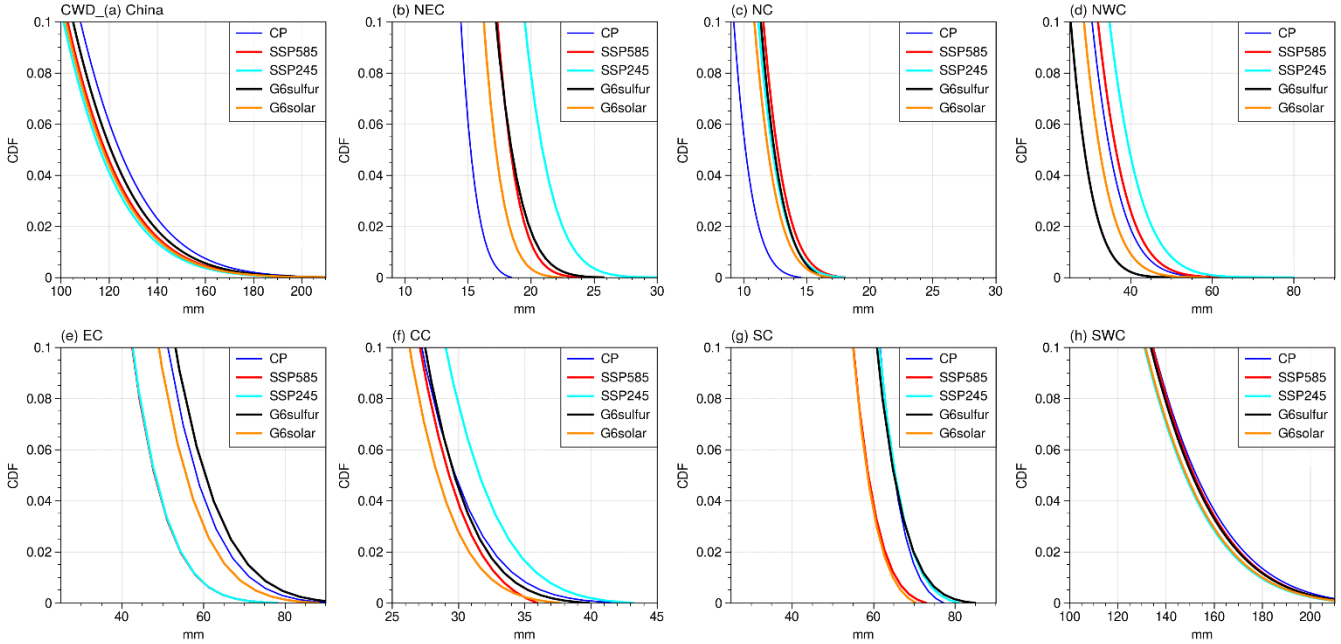

Figure 9. Same as Figure 6, but for CWD in China and 7 subregions.

In summary, CWD under SSP5-8.5 and SSP2-4.5 scenarios does not consistently exhibit simultaneously increases or decreases across all regions. CWD will significantly increase in QTP, and decrease in north China (almost in mid-latitudes, north of 30°N) but not serious in the future. The maximum increase occurs is in SWC, SAI effectively ameliorates the decrease of CWD under SSP5-8.5 in southeast QTP (from about 90°E - 100°E). G6sulfur yields statistically similar outcome to that of SSP2-4.5 in NC and SC. SRM strategies yields results in R50mm nearly identical to those of the SSP2-4.5 scenario. As the global mean temperature targets of G6sulfur, G6solar and SSP2-4.5 are nominally identical, this suggests that it is the global mean temperature change that is the dominant factor in driving changes in extreme precipitation.

3.2.2 Dry extreme changes

As for extreme wet indices, extreme dry conditions also occur in China, especially in north-western regions (Wang et al., 2017). The focus is on DD and CDD to study these changes and explore the impact of SAI.

For DD, the ensemble mean of UKESM simulations projects a significant increase in most of southern China (east of SWC, SC, and south of CC, EC) and a small part of western Xinjiang province (Fig.10a) for the SSP5-8.5 scenario (2071-2100) relative to the control period (1981-2010). The largest increase, reaching up to 40 days, is observed in Fuzhou and Taiwan (southeast SC, near 120° E, 25°N). Decreases in DD are observed in northern and west China, including NEC, NC, NWC,

west of SWC and north of CC, EC. Similar changes with smaller magnitudes are also observed under the SSP2-4.5 scenario (Fig.10b) and G6solar (Fig.10d). It is worth noting that, in comparison to the other three experiments, G6sulfur results in the most substantial increase in DD in western NWC (Fig.7c, Kunlun Mountains) in the future, indicating that G6sulfur exacerbates drought conditions in Kunlun Mountains. This may be related to topography and slope, both of which play important roles in glacier change in the Kunlun Mountains (Niu et al., 2023).

Under SSP5-8.5 warming conditions (Fig.10e), there is a significant CDD decrease in north-western and northern China, with the most significant decrease in NWC, consistent with Xu et al., (2019). This implies that ignoring rising temperatures seems to mitigate dry conditions (Xu et al., 2022a). In line with prior studies, there are notable north-south CDD variation in China (Feng et al., 2011).

The figure shows increased CDD in southern regions (along the middle and lower Yangtze River, south and parts of southwest China) but not significantly, hinting at potential increased droughts in southern China (Feng et al., 2011). These results also align with the predicted decrease in the north and increase in the south in CDD by RegCM4 (Ji and Kang, 2015) and PRECIS (Meng et al., 2021) models. Smaller CDD changes are observed in most regions under SSP2-4.5 (Fig.10f), G6sulfur (Fig.10g) and G6solar (Fig.10h). It worth noting that G6sulfur shows a slight future increase in western China (Tarim Basin).

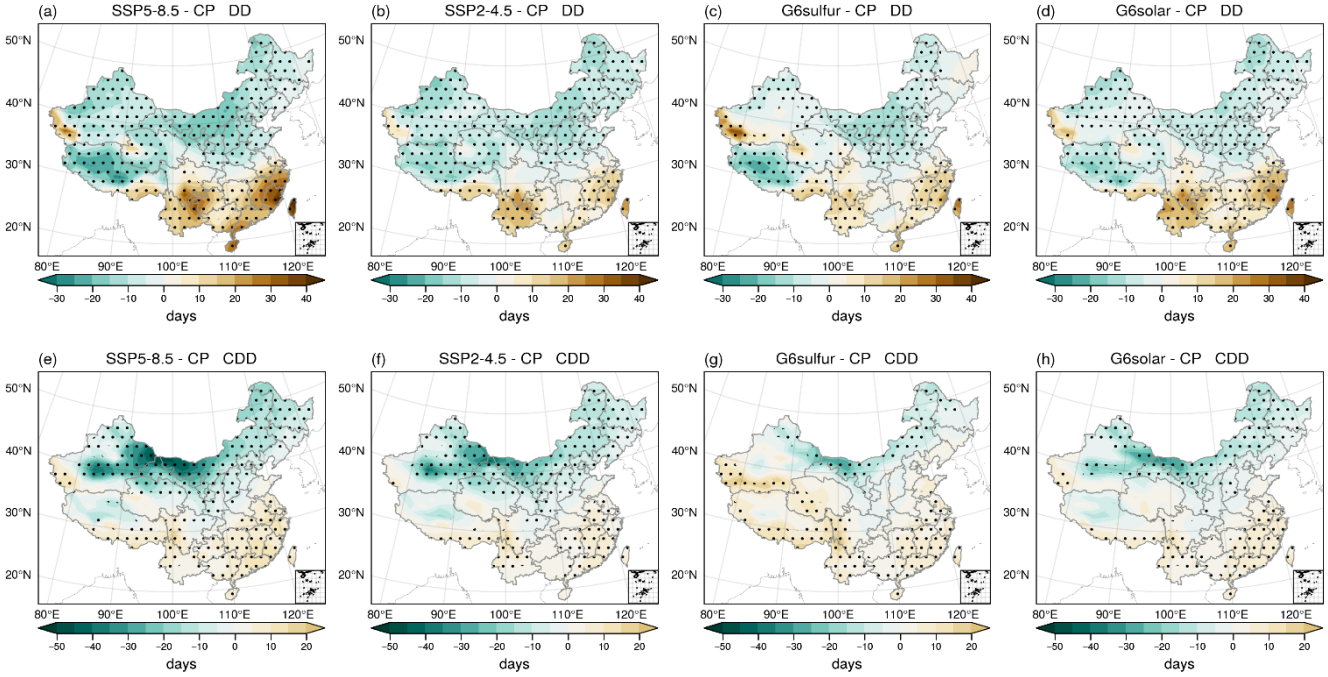

Figure 10. Same as Figure 4, but for (a-d) DD (days) and (e-h) CDD (days).

Fig.11 shows the impact of SAI on DD and CDD distribution in comparison to G6sulfur and other experiments. G6sulfur increases DD in northern and northwest China compared to SSP5-8.5 (Fig.11a), albeit mitigating the DD in a warmer climate (Fig.10c). Compared to SSP2-4.5 (Fig.11b), G6sulfur leads to a further increase in western China near 35°N, up to 25 days. However, G6sulfur reduces dry climate in the south China compared to other experiments, despite an increased drought risk (as seen in Fig.10a-d). Comparisons confirm that G6sulfur increases CDD in most inland areas of China compared to SSP5-8.5 (Fig.11d), Only a few coastal areas show a reduction. G6sulfur increases the CDD almost across the entire China when compared to SSP2-4.5 (Fig.11e) and G6solar (Fig.11f).

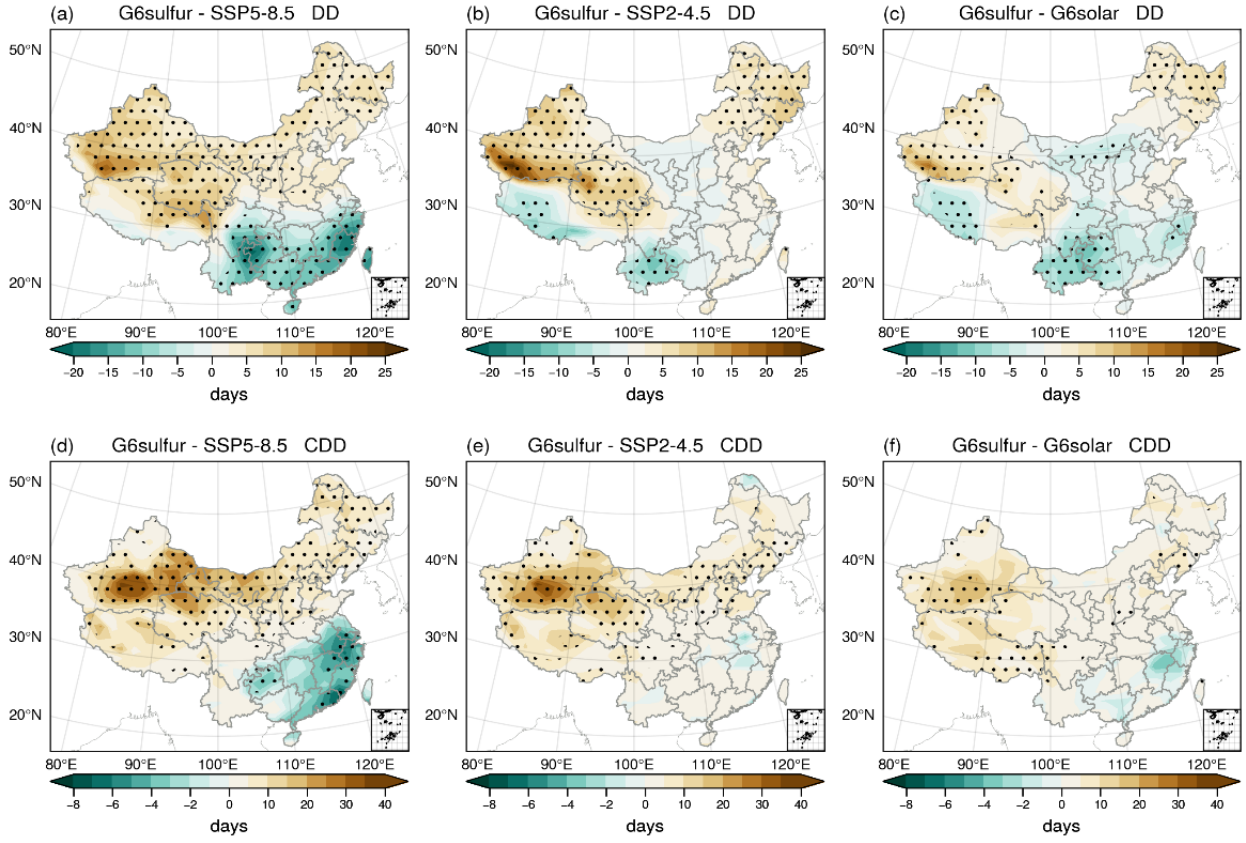

Figure 11. Same as Figure 5, but for (a-c) DD (days) and (d-f) CDD (days).

The tail of the DD CDFs in control period (blue) is consistently shifts to the right compared to the other lines in NEC, NC, and NWC (Fig.12(a2) - (a4)), which corresponds to the declining trend (green shaded areas) in northern China as shown in Fig.10a-d. As shown in Table 3, the DD is positive in the SC region, meaning G6sulfur effectively lowers the threshold for extreme

DD events compared to SSP5-8.5. This suggests that the SAI is more effective for DD maximum in the humid region. The black line surpasses the other three experiments in NWC, which explains the maximum increase value along Kunlun Mountains in NWC in Fig.10a-d and Fig.11a-c.

The blue line surpasses the other four lines in NEC, NC and NWC, clarifying the decrease of CDD in the northern regions as evident in Fig.10e-h, signifying a reduced drought risk in northern China in the future. Conversely, the red line consistently stays to the left, while the black line is positioned to the right compared to the other G6 experiment lines. This suggests that G6sulfur and G6solar increase the drought risk when compared to the SSP5-8.5 scenario in northern regions, and the effect of G6sulfur is more pronounced than that of G6solar. However, the distance between black and other G6 experiments lines is wider in NWC than in other regions, indicating the maximum increase in CDD under G6sulfur in NWC. This corresponds to the maximum differences in NWC in Fig.11d-f. The positive value in Table 3 of the CDD index in the SC and SWC regions in Table 3 indicates that G6sulfur notably closes the threshold of CP extreme CDD events compared to SSP5-8.5, thereby approaching drought extremes of CP in these regions. This suggests that G6sulfur has the potential to mitigate the CDD extremes. The ameliorating effect of DD and CDD compared to SSP5-8.5 in the SC region under G6sulfur may be related to the strengthening of the anti-cyclonic circulation associated with the subtropical gyre, which appears to increase under G6 compared to SSP5-8.5 (Liang and Haywood, 2023). This intensification results in an increased inflow of moist air from the ocean at 850hPa and a greater supply of moisture to the southern region of the area.

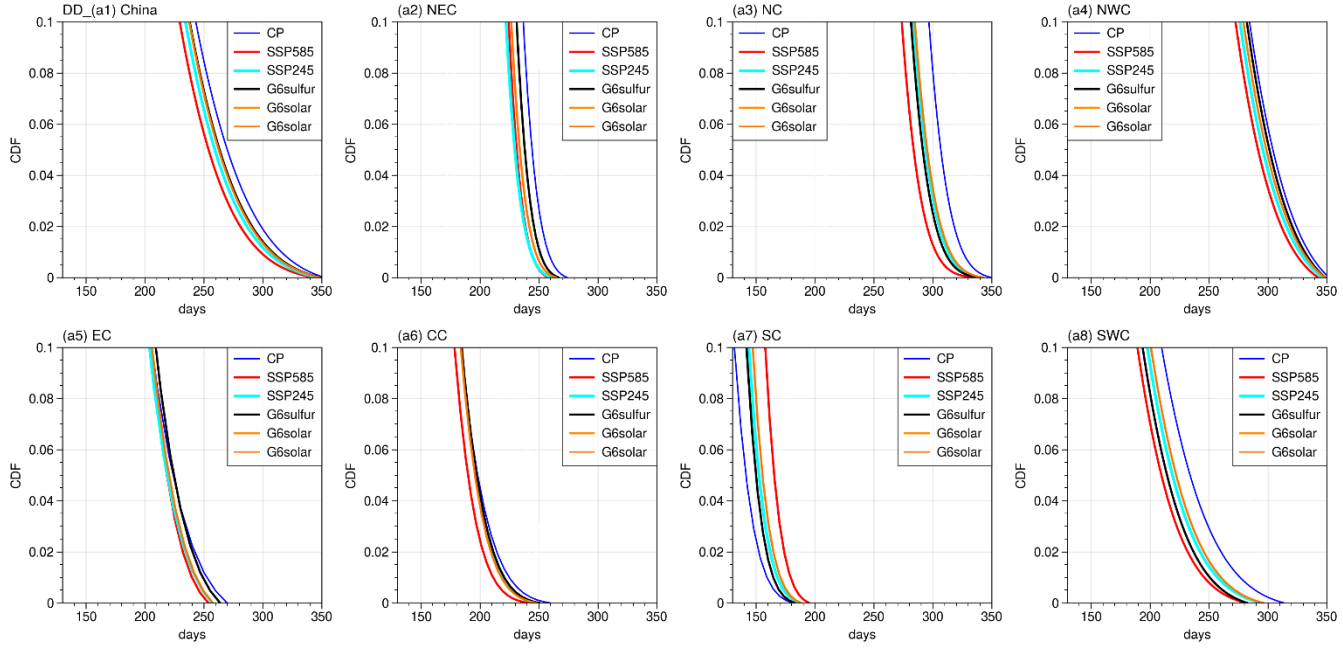

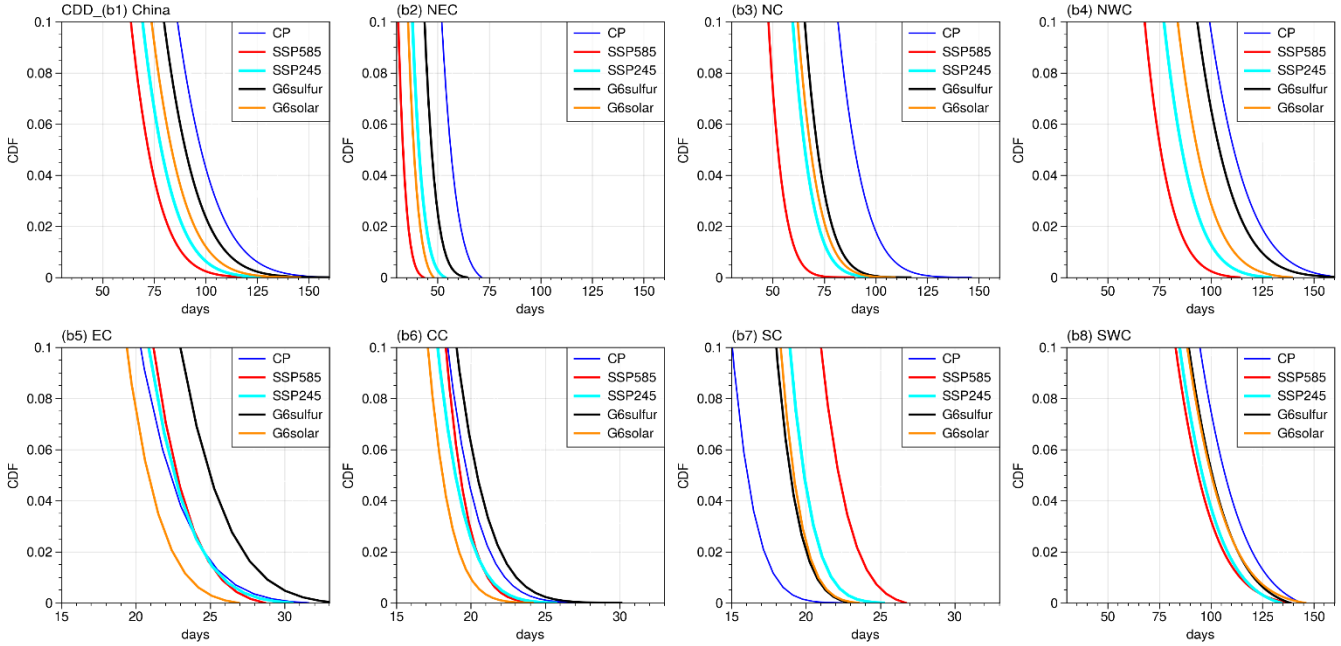

Figure 12. Same as Figure 6, but for DD (a1-a8) and CDD (b1-b8) in China and 7 subregions.

In summary, both DD and CDD projected increase in the south and southeast China but decrease in the north and northwest regions by the end of the 21st century in the four scenarios. This reflects a potential decrease in drought risk in northwest regions and an increase in extreme drought events in low-latitude southeast coastal areas in the future according to four G6 simulations. Changes in precipitation will affect soil moisture, thereby influencing evapotranspiration (ET) and ultimately precipitation patterns. Assessing whether changes in DD and CDD affect drought risk also requires consideration of variations in ET and soil moisture (Cheng et al., 2019; Dagon and Schrag, 2016). Furthermore, solar radiation management (SRM) may increase drought risk in northern regions (NEC, NC, and NWC).

4. Summary and discussion

In this study, based on simulations of the UKESM1, the effects of SAI on precipitation and the related extreme metrics are assessed over different sub-regions in China by comparing the results among different scenarios. We found that, under future emission scenarios (SSP5-8.5 and SSP2-4.5), most of the sub-regions in China are projected to experience increased precipitation and extreme wet climate events by the end of 21st century, compared to the control period (1981-2010), particularly in the eastern and south-eastern coastal areas. Both the G6sulfur and G6solar show remarkable ameliorated changes in extreme rainfall intensity and frequency, and may abate most of the detrimental extremes that are evident under the SSP5-8.5 scenario. In general, the effects of the SRM experiments are similar to that of the SSP2-4.5. This suggests that the

effects of SAI are encouraging, and can be seen as an effective option for mitigating flooding events, especially in the populated southeast areas. However, extreme drought events show an increase in some regions such as the north and northwest China compared with SSP5-8.5, implying the SRM may not suitable for addressing drought risk in these regions. All the findings in our paper extend the current understating of extreme hydrological responses to climate change and SAI in China. The regional analysis presents new insights into identifying the vulnerable areas under hydrological changes and how they may benefit from the SRM.

As this study is solely focused on the precipitation and relevant extreme events based on the models, we cannot take socio-economic, biological, and other factors into account. Although many studies have also focused on areas such as crops (Cheng et al., 2019) and important modes of natural variability (Jones et al., 2020), they are mostly targeted on a wider and global scale, more regional analysis on China still requires future research. Also, the climate models and data remain uncertain, indicating the continuous improvements are needed in models for simulations in deterring the future pathways of climate change and SRM. In addition, it should be noted that, owing to the second-order nature of the changes in climate extremes when compared to SSP2-4.5 (i.e. a relatively small signal to noise when compared to those from SSP5-8.5), that the analysis is very dependent on the model used in the analysis (UKESM1); other models may produce significantly different results. Additionally, reducing the solar constant within climate models also triggers a dynamic reaction in the stratosphere (Bednarz et al., 2022). It is therefore crucial to perform similar analyses with other state-of-the-art climate models to elucidate the robustness of the results, and to inform policymakers of any potential detrimental influences of SRM.

While the general amelioration of precipitation changes under SAI might seem a somewhat obvious conclusion owing to the spin-down of the hydrological cycle under cooler temperatures (e.g. Tilmes et al, 2013), other studies have shown large-scale climatic shifts in key modes of climate variability that impact precipitations. For example, Haywood et al. (2013) and Jones et al. (2017) have modelled significant detrimental impacts on Sahelian precipitation and north Atlantic hurricane frequency under non-judicious SAI implementation owing to large-scale shifts in the Inter-Tropical Convergence Zone. Multi-model SAI simulations Jones et al. (2020, 2021) have shown detrimental impacts on the North Atlantic Oscillation leading to rainfall deficits over the Iberian Peninsula above and beyond those evident in SSP5-8.5. Similarly, recent simulations of non-judicious deployment of an alternate SRM technique, that of marine cloud brightening, locked the climate into an extremely strong permanent La-Nina-like phase with associated detrimental impacts on sea-level rise over low-lying South Pacific islands (Haywood et al., 2023). It appears that, over large areas of China, any changes in detrimental extremes in precipitation are second order when compared to the benefits associated with reducing global mean temperatures.

To conclude, it appears that changes in precipitation extremes related to flooding over the bulk of China that are induced under climate change may be abated by SRM, but changes in dry days relating to drought are likely to be enhanced. Large-scale shifts in precipitation patterns associated with changes in atmospheric dynamics noted in other SRM studies using climate

models developed by the Hadley Centre (e.g. HadGEM2, UKESM1; Haywood et al., 2013, 2023; Jones et al., 2017; Jones et al., 2020; 2021) do not appear to impact the bulk of China. Based on the same set of simulations as this paper, the study by Liang and Haywood (2023) demonstrated apparent side-effects of SRM as the simulated SAI scenario exacerbates the weakening the subtropical westerly jet and further enhance the mid-latitude precipitation over China by modulating atmospheric rivers over East Asia. Of course, we stress that the results from these simulations are model specific and further work with other models needs to be performed to understand the robustness of these conclusions more generally.

Code and data availability

All the UKESM1 model data for the SSP5-8.5, SSP2-4.5, GeoMIP G6sulfur and GeoMIP G6solar scenarios used in this work are available from the Earth System Grid Federation (WCRP, 2022; https://esgf-node.llnl.gov/projects/cmip6). The APHRODITE data have been downloaded from their official website, which is managed by the Data Integration and Analysis System (DIAS, 2022; https://search.diasjp.net/en/dataset/APHRO_MA).

Supplement

The supplement related to this article is available online at:

Author contributions

The majority of this work was completed when OW was visiting the University of Exeter in the UK under a scholarship from the China Scholarship Council. JL and JH devised the experiment, led the analysis. OW wrote the paper with contributions from all the co-authors.

Competing interests

The contact authors have declared that neither of the authors has any competing interests.

Disclaimer

Publisher's note: Copernicus Publications remains neutral with regard to jurisdictional claims in published maps and institutional affiliations.

Acknowledgements

We are grateful to the University of Exeter for providing the academic platform for this study and the Met Office for doing the numerical calculations in this work. The authors thank Andy Jones, for help with running the G6sulfur and G6solar experiments.

Reference

Apurv, T., Mehrotra, R., Sharma, A., Goyal, M. K., and Dutta, S.: Impact of climate change on floods in the Brahmaputra basin using CMIP5 decadal predictions, J. Hydrol., 527, 281-291, https://doi.org/10.1016/j.jHydrol.2015.04.056, 2015.

Archibald, A. T., O'Connor, F. M., Abraham, N. L., Archer-Nicholls, S., Chipperfield, M. P., Dalvi, M., Folberth, G. A., Dennison, F., Dhomse, S. S., and Griffiths, P. T.: Description and evaluation of the UKCA stratosphere–troposphere chemistry scheme (StratTrop vn 1.0) implemented in UKESM1, Geosci. Model Dev., 13, 1223-1266, https://doi.org/10.5194/gmd-13-1223-2020, 2020.

Bednarz, E. M., Visioni, D., Banerjee, A., Braesicke, P., Kravitz, B., and MacMartin, D. G.: The Overlooked Role of the Stratosphere Under a Solar Constant Reduction, Geophys. Res. Lett., 49, e2022GL098773, https://doi.org/10.1029/2022GL098773, 2022.

Bluth, G. J., Doiron, S. D., Schnetzler, C. C., Krueger, A. J., and Walter, L. S.: Global tracking of the SO2 clouds from the June, 1991 Mount Pinatubo eruptions, Geophys Res Lett., 19, 151-154, https://doi.org/10.1029/91GL02792, 1992.

CDF vs PDF: What's the Difference?: https://www.analyticsvidhya.com/blog/2023/07/cdf-vs-pdf/, last access: 15 November 2023.

CDP. 2023 China Floods.: The summer of 2023 has seen unprecedented flooding across China as monsoon season, typhoons and intense rainfall have battered the country. https://disasterphilanthropy.org/disasters/2023-china-floods/, last access: 10 November 2023.

Cheng, W., MacMartin, D. G., Dagon, K., Kravitz, B., Tilmes, S., Richter, J. H., Mills, M. J., and Simpson, I. R.: Soil moisture and other hydrological changes in a stratospheric aerosol geoengineering large ensemble, J. Geophys. Res.-Atmos., 124, 12773-12793, https://doi.org/10.1029/2018JD030237, 2019.

Deng, L., Feng, J., Zhao, Y., Bao, X., Huang, W., Hu, H., and Duan, Y.: The remote effect of binary Typhoon Infa and Cempaka on the "21.7" heavy rainfall in Henan Province, China, J. Geophys. Res.-Atmos., 127, e2021JD036260, https://doi.org/10.1029/2021JD036260, 2022.

Dong, B., Xia, J., Li, Q., and Zhou, M.: Risk assessment for people and vehicles in an extreme urban flood: Case study of the "7.20" flood event in Zhengzhou, China, Int. J. Disaster Risk Reduct., 80, 103205, https://doi.org/10.1016/j.ijdrr.2022.103205, 2022.

Eyring, V., Bony, S., Meehl, G. A., Senior, C. A., Stevens, B., Stouffer, R. J., and Taylor, K. E.: Overview of the Coupled Model Intercomparison Project Phase 6 (CMIP6) experimental design and organization, Geosci. Model Dev., 9, 1937-1958, https://doi.org/10.5194/gmd-9-1937-2016, 2016.

Feng, L., Zhou, T., Wu, B., Li, T., and Luo, J.-J.: Projection of future precipitation change over China with a high-resolution global atmospheric model, Adv. Atmos. Sci., 28, 464-476, https://doi.org/10.1007/s00376-010-0016-1, 2011.

Frich, P., Alexander, L. V., Della-Marta, P., Gleason, B., Haylock, M., Tank, A. K., and Peterson, T.: Observed coherent changes in climatic extremes during the second half of the twentieth century, Clim. Res., 19, 193-212, https://doi.org/10.3354/cr019193, 2002.

Haywood, J. M., Jones, A., and Jones, G. S.: The impact of volcanic eruptions in the period 2000–2013 on global mean temperature trends evaluated in the HadGEM2-ES climate model, Atmos. Sci. Lett., 15, 92-96, https://doi.org/10.1002/asl2.471, 2014.

Haywood, J. M., Jones, A., Johnson, B. T., and McFarlane Smith, W.: Assessing the consequences of including aerosol absorption in potential stratospheric aerosol injection climate intervention strategies, Atmos. Chem. Phys., 22, 6135-6150, https://doi.org/10.5194/acp-22-6135-2022, 2022.

Held, I. M. and Soden, B. J.: Robust responses of the hydrological cycle to global warming, J. Climate., 19, 5686-5699, https://doi.org/10.1175/JCLI3990.1, 2006.

Huang, R., Chen, J., and Huang, G.: Characteristics and variations of the East Asian monsoon system and its impacts on climate disasters in China, Adv. Atmos. Sci., 24, 993-1023, https://doi.org/10.1007/s00376-007-0993-x, 2007.

Imai, Y., Meyer, K. J., Iinishi, A., Favre-Godal, Q., Green, R., Manuse, S., Caboni, M., Mori, M., Niles, S., and Ghiglieri, M.: A pause in Southern Hemisphere circulation trends due to the Montreal Protocol, Nature, 579(7800), 544-548, https://doi.org/10.1038/s41586-020-2120-4, 2020.

IPCC, C. C. The Physical Science Basis. Contribution of Workin g Group I to the 6th Assessment Report, 2021.

IPCC – Intergovernmental Panel on Climate Change: Global warming of 1.5 ◦C, in: An IPCC Special Report on the impacts of global warming of 1.5 ◦C above pre-industrial levels and related global greenhouse gas emission pathways, in the context of strengthening the global response to the threat of climate change, sustainable development, and efforts to eradicate poverty, edited by: Masson-Delmotte, V., Zhai, P., Pörtner, H. O., Roberts, D., Skea, J., Shukla, P. R., Pirani, A., Moufouma-Okia, W., Péan, C., Pidcock, R., Connors, S., Matthews, J. B. R., Chen, Y., Zhou, X., Gomis, M. I., Lonnoy, E., Maycock, T., Tignor, M., and Waterfield, T., https://www.ipcc.ch/sr15/ (last access: 22 September 2022), 2018.

Irvine, P. J., Kravitz, B., Lawrence, M. G., and Muri, H.: An overview of the Earth system science of solar geoengineering, WIREs Climate Change, 7, 815–833, https://doi.org/10.1002/wcc.423, 2016.

Ji, D., Fang, S., Curry, C. L., Kashimura, H., Watanabe, S., Cole, J. N., Lenton, A., Muri, H., Kravitz, B., and Moore, J. C.: Extreme temperature and precipitation response to solar dimming and stratospheric aerosol geoengineering, Atmos. Chem. Phys., 18, 10133-10156, https://doi.org/10.5194/acp-18-10133-2018, 2018.

Ji, Z. and Kang, S.: Evaluation of extreme climate events using a regional climate model for China, Int. J. Climatol., 35, 888-902, https://doi.org/10.1002/joc.4024, 2015.

Jia, H., Chen, F., Pan, D., Du, E., Wang, L., Wang, N., and Yang, A.: Flood risk management in the Yangtze River basin—Comparison of 1998 and 2020 events, Int. J. Disaster Risk Reduct., 68, 102724, https://doi.org/10.1016/j.ijdrr.2021.102724, 2022.

Jones, A. C., Hawcroft, M. K., Haywood, J. M., Jones, A., Guo, X., and Moore, J. C.: Regional climate impacts of stabilizing global warming at 1.5 K using solar geoengineering, Earth's Future, 6, 230-251, https://doi.org/10.1002/2017EF000720, 2018.

Jones, A., Haywood, J. M., Jones, A. C., Tilmes, S., Kravitz, B., and Robock, A.: North Atlantic Oscillation response in GeoMIP experiments G6solar and G6sulfur: why detailed modelling is needed for understanding regional implications of solar radiation management, Atmos. Chem. Phys., 21, 1287–1304, https://doi.org/10.5194/acp-21-1287-2021, 2021.

Kravitz, B., Robock, A., Boucher, O., Schmidt, H., Taylor, K. E., Stenchikov, G., and Schulz, M.: The geoengineering model intercomparison project (GeoMIP), Atmos. Sci. Lett., 12, 162-167, 2011.

595 Kravitz, B., Caldeira, K., Boucher, O., Robock, A., Rasch, P. J., Alterskjaer, K., Karam, D. B., Cole, J. N., Curry, C. L., and Haywood, J. M.: Climate model response from the geoengineering model intercomparison project (GeoMIP), J. Geophys. Res.-Atmos., 118, 8320-8332, https://doi.org/10.1002/jgrd.50646, 2013.

Kravitz, B., Robock, A., Tilmes, S., Boucher, O., English, J. M., Irvine, P. J., Jones, A., Lawrence, M. G., MacCracken, M., 600 and Muri, H.: The geoengineering model intercomparison project phase 6 (GeoMIP6): Simulation design and preliminary results, Geosci. Model Dev., 8, 3379-3392, https://doi.org/10.5194/gmd-8-3379-2015, 2015.

Klein Tank, A. M. G., Zwiers, F. W., and Zhang, X.: Guidelines on Analysis of extremes in a changing climate in support of informed decisions for adaptation, in: Climate Data and Monitoring, (WCDMP-No. 72; p. 52), World Meteorological 605 Organization, https://library.wmo.int/doc_num.php?explnum_id=9419 (last access: 24 August 2022), 2009.

Lai, S., Xie, Z., Bueh, C., and Gong, Y.: Fidelity of the APHRODITE dataset in representing extreme precipitation over Central Asia, Adv. Atmos. Sci., 37, 1405-1416, https://doi.org/10.1007/s00376-020-0098-3, 2020.

610 Lee, H., Muri, H., Ekici, A., Tjiputra, J., and Schwinger, J.: The response of terrestrial ecosystem carbon cycling under different aerosol-based radiation management geoengineering, Earth Syst. Dynam., 12, 313-326, https://doi.org/10.5194/esd-12-313-2021, 2021.

Li, S., Jiang, D., Lian, Y., and Yao, Y.: Interdecadal variations of cold air activities in Northeast China during springtime, J. 615 Meteorol. Res., 30, 645-661, https://doi.org/10.1007/s13351-016-5912-6, 2016.

Liang, J. and Haywood, J.: Future changes in atmospheric rivers over East Asia under stratospheric aerosol intervention, Atmos. Chem. Phys., 23, 1687-1703, https://doi.org/10.5194/acp-23-1687-2023, 2023.

620 Liang, J., Meng, C., Wang, J., Pan, X., and Pan, Z.: Projections of mean and extreme precipitation over China and their resolution dependence in the HighResMIP experiments, Atmos. Res., 293, 106932, https://doi.org/10.1016/j.atmosres.2023.106932, 2023.

Liu, Z., Lang, X., and Jiang, D.: Impact of stratospheric aerosol injection geoengineering on the summer climate over East 625 Asia, J. Geophys. Res.-Atmos., 126, e2021JD035049, https://doi.org/10.1029/2021JD035049, 2021.

Liu, Z., Lang, X., Miao, J., and Jiang, D.: Impact of Stratospheric Aerosol Injection on the East Asian Winter Monsoon, Geophys. Res. Lett., 50, e2022GL102109, https://doi.org/10.1029/2022GL102109, 2023.

McLandress, C., Shepherd, T. G., Scinocca, J. F., Plummer, D. A., Sigmond, M., Jonsson, A. I., and Reader, M. C.: Separating the dynamical effects of climate change and ozone depletion. Part II: Southern Hemisphere troposphere, J. Climate., 24, 1850-1868, https://doi.org/10.1175/2010JCLI3958.1, 2011.

Meinshausen, M., Nicholls, Z. R., Lewis, J., Gidden, M. J., Vogel, E., Freund, M., Beyerle, U., Gessner, C., Nauels, A., and Bauer, N.: The shared socio-economic pathway (SSP) greenhouse gas concentrations and their extensions to 2500, Geosci. Model Dev., 13, 3571-3605, https://doi.org/10.5194/gmd-13-3571-2020, 2020.

Meng, C., Zhang, L., Gou, P., Huang, Q., Ma, Y., Miao, S., Ma, W., and Xu, Y.: Assessments of future climate extremes in China by using high-resolution PRECIS 2.0 simulations, Theor. Appl. Climatol., 145, 295-311, https://doi.org/10.1007/s00704-021-03618-9, 2021.

Mulcahy, J. P., Jones, C., Sellar, A., Johnson, B., Boutle, I. A., Jones, A., Andrews, T., Rumbold, S. T., Mollard, J., Bellouin, N., Johnson, C. E., Williams, K. D., Grosvenor, D. P., and McCoy, D. T.: Improved Aerosol Processes and Effective Radiative Forcing in HadGEM3 and UKESM1, J. Adv. Model. Earth Sy., 10, 2786–2805, https://doi.org/10.1029/2018MS001464, 2018.

Niemeier, U., Schmidt, H., Alterskjær, K., and Kristjánsson, J.: Solar irradiance reduction via climate engineering: Impact of different techniques on the energy balance and the hydrological cycle, J. Geophys. Res.-Atmos., 118, 11,905-911,917, https://doi.org/10.1002/2013JD020445, 2013.

Niu, S., Sun, M., Wang, G., Wang, W., Yao, X., and Zhang, C.: Glacier Change and Its Influencing Factors in the Northern Part of the Kunlun Mountains, Remote Sens., 15, 3986, https://doi.org/10.3390/rs15163986, 2023.

O'neill, B., Tebaldi, C., Van Vuuren, D., Eyring, V., Friedlingstein, P., Hurtt, G., Knutti, R., Kriegler, E., Lamarque, J., and Lowe, J.: The Scenario Model Intercomparison Project (ScenarioMIP) for CMIP6, Geosci. Model Dev., 9, 3461–3482, https://doi.org/10.5194/gmd-9-3461-2016, 2016.

Peng, Y., Zhao, X., Wu, D., Tang, B., Xu, P., Du, X., and Wang, H.: Spatiotemporal variability in extreme precipitation in China from observations and projections, Water, 10, 1089, https://doi.org/10.3390/w10081089, 2018.

Pinto, I., Jack, C., Lennard, C., Tilmes, S., and Odoulami, R. C.: Africa's climate response to solar radiation management with stratospheric aerosol, Geophys. Res. Lett., 47, e2019GL086047, https://doi.org/10.1029/2019GL086047, 2020.

Plazzotta, M., Séférian, R., and Douville, H.: Impact of Solar Radiation Modification on Allowable CO2 Emissions: What Can We Learn From Multimodel Simulations?, Earth's Future, 7, 664–676, https://doi.org/10.1029/2019EF001165, 2019.

Qi, Y., Yu, H., Fu, Q., Chen, Q., Ran, J., and Yang, Z.: Future changes in drought frequency due to changes in the mean and shape of the PDSI probability density function under RCP4. 5 scenario, Front Earth Sci, 10, 386, https://doi.org/10.3389/feart.2022.857885, 2022.

Qin, P. and Xie, Z.: Detecting changes in future precipitation extremes over eight river basins in China using RegCM4 downscaling, J. Geophys. Res.-Atmos., 121, 6802-6821, https://doi.org/10.1002/2016JD024776, 2016.

Rana, A., Madan, S., and Bengtsson, L.: Performance evaluation of regional climate models (RCMs) in determining precipitation characteristics for Gothenburg, Sweden, Hydrol. Res., 45, 703-714, https://doi.org/10.2166/nh.2013.160, 2013.

Rao, C., Chen, G., and Ran, L.: Effects of Typhoon In-Fa (2021) and the Western Pacific Subtropical High on an Extreme Heavy Rainfall Event in Central China, J. Geophys. Res.-Atmos., 128, e2022JD037924, https://doi.org/10.1029/2022JD037924, 2023.

REUTERS: FACTBOX Impact of floods in China after Typhoon Doksur, https://www.reuters.com/world/asia-pacific/impact-floods-china-after-typhoon-doksuri-2023-08-11/, last access: 11 November 2023.

Robock, A.: Volcanic eruptions and climate, Rev. Geophys., 38, 191-219, https://doi.org/10.1029/1998RG000054, 2000.Schmidt, A., Mills, M. J., Ghan, S., Gregory, J. M., Allan, R. P., Andrews, T., Bardeen, C. G., Conley, A., Forster, P. M., and Gettelman, A.: Volcanic radiative forcing from 1979 to 2015, J. Geophys. Res.-Atmos., 123, 12491-12508, https://doi.org/10.1029/2018JD028776, 2018.

Self, S., Zhao, J.-X., Holasek, R. E., Torres, R. C., and King, A. J.: The atmospheric impact of the 1991 Mount Pinatubo eruption, in: Fire and Mud: Eruptions and lahars of Mount Pinatubo, Philippines, University of Washington Press, 1996.Sellar, A., Jones, C. G., Mulcahy, J. P., Tang, Y., Yool, A., Wiltshire, A., O'Connor, F. M., Stringer, M., Hill, R., Palmieri, J., Woodward, S., de Mora, L., Kuhlbrodt, T., Rumbold, S., Kelley, D. I., Ellis, R., Johnson, C. E., Walton, J., Abraham, N. L., Andrews, M. B., Andrews, T., Archibald, A. T., Berthou, S., Burke, E., Blockley, E., Carslaw, K., Dalvi, M., Edwards, J., Folberth, G. A., Gedney, N., Griffiths, P. T., Harper, A. B., Hendry, M. A., Hewitt, A. J., Johnson, B., Jones, A., Jones, C. D., Keeble, J., Liddicoat, S., Morgenstern, O., Parker, R. J., Predoi, V., Robertson, E., Siahaan, A., Smith, R. S., Swaminathan, R., Woodhouse, M., Zeng, G., and Zerroukat, M.: UKESM1: Description and evaluation of the UK Earth System Model, J. Adv. Model. Earth Sy., 11, 4513–4558, https://doi.org/10.1029/2019MS001739, 2019.

Simpson, I. S., S.Tilmes, Richter, J. H., Kravitz, B., MacMartin, D. G., Mills, M. J., Fasullo, J. T., and Pendergrass, A. G.: The regional hydroclimate response to stratospheric sulfate geoengineering and the role of stratospheric heating, J. Geophys. Res.-Atmos., 124, 12587–12616, 2019.

Soden, B. J., Wetherald, R. T., Stenchikov, G. L., and Robock, A.: Global cooling after the eruption of Mount Pinatubo: A test of climate feedback by water vapor, Science, 296, 727-730, https://doi.org/10.1126/science.296.5568.727, 2002.

Stenchikov, G. L., Kirchner, I., Robock, A., Graf, H. F., Antuna, J. C., Grainger, R. G., Lambert, A., and Thomason, L.: Radiative forcing from the 1991 Mount Pinatubo volcanic eruption, J. Geophys. Res.-Atmos., 103, 13837-13857, https://doi.org/10.1029/98JD00693, 1998.

Storkey, D., Blaker, A. T., Mathiot, P., Megann, A., Aksenov, Y., Blockley, E. W., Calvert, D., Graham, T., Hewitt, H. T., and Hyder, P.: UK Global Ocean GO6 and GO7: A traceable hierarchy of model resolutions, Geosci. Model Dev., 11, 3187-3213, https://doi.org/10.5194/gmd-11-3187-2018, 2018.

Sui, Y., Lang, X., and Jiang, D.: Projected signals in climate extremes over China associated with a 2 C global warming under two RCP scenarios, Int. J. Climatol., 38, e678-e697, https://doi.org/10.1002/joc.5399, 2018.

Sunilkumar, K., Yatagai, A., and Masuda, M.: Preliminary evaluation of GPM-IMERG rainfall estimates over three distinct climate zones with APHRODITE, Earth. Sp. Sci., 6, 1321-1335, https://doi.org/10.1029/2018EA000503, 2019.

Tabari, H.: Climate change impact on flood and extreme precipitation increases with water availability. Sci. Rep., 10: 13768, https://doi.org/10.1038/s41598-020-70816-2, 2020.

Tang, B., Hu, W., and Duan, A.: Future projection of extreme precipitation indices over the Indochina Peninsula and South China in CMIP6 models, J. Climate., 34, 8793-8811, https://doi.org/10.1175/JCLI-D-20-0946.1, 2021.

Tew, Y. L., Tan, M. L., Liew, J., Chang, C. K., & Muhamad, N.: A review of the effects of solar radiation management on hydrological extremes, Earth Environ., 1238, 1, https://doi.org/10.1088/1755-1315/1238/1/012030, 2023.

Tung, Y.-S., Wang, C.-Y., Weng, S.-P., and Yang, C.-D.: Extreme index trends of daily gridded rainfall dataset (1960–2017) in Taiwan, Terr. Atmos. Oceanic Sci., 33, 8, https://doi.org/10.1007/s44195-022-00009-z, 2022.

Tye, M. R., Dagon, K., Molina, M. J., Richter, J. H., Visioni, D., Kravitz, B., and Tilmes, S.: Indices of extremes: geographic patterns of change in extremes and associated vegetation impacts under climate intervention, Earth Syst. Dynam., 13, 1233–1257, https://doi.org/10.5194/esd-13-1233-2022, 2022.

Visioni, D., Jones, A., Haywood, J., Séférian, R., Nabat, P., Boucher, O., Bednarz, E. M., and Niemeier, U.: Stratospheric ozone response to sulfate aerosol and solar dimming climate interventions based on the G6 Geoengineering Model Intercomparison Project (GeoMIP) simulations, Atmos. Chem. Phys., 22, 4557-4579, https://doi.org/10.5194/acp-22-4557-2022, 2022.

Visioni, D., MacMartin, D. G., Kravitz, B., Boucher, O., Jones, A., Lurton, T., Martine, M., Mills, M. J., Nabat, P., and Niemeier, U.: Identifying the sources of uncertainty in climate model simulations of solar radiation modification with the G6sulfur and G6solar Geoengineering Model Intercomparison Project (GeoMIP) simulations, Atmos. Chem. Phys., 21, 10039-10063, https://doi.org/10.5194/acp-21-10039-2021, 2021.

Walters, D., Baran, A. J., Boutle, I., Brooks, M., Earnshaw, P., Edwards, J., Furtado, K., Hill, P., Lock, A., Manners, J., Morcrette, C., Mulcahy, J., Sanchez, C., Smith, C., Stratton, R., Tennant, W., Tomassini, L., Van Weverberg, K., Vosper, S., Willett, M., Browse, J., Bushell, A., Carslaw, K., Dalvi, M., Essery, R., Gedney, N., Hardiman, S., Johnson, B., Johnson, C., Jones, A., Jones, C., Mann, G., Milton, S., Rumbold, H., Sellar, A., Ujiie, M., Whitall, M., Williams, K., and Zerroukat, M.: The Met Office Unified Model Global Atmosphere 7.0/7.1 and JULES Global Land 7.0 configurations, Geosci. Model Dev., 12, 1909–1963, https://doi.org/10.5194/gmd-12-1909-2019, 2019

Wang, X., Pang, G., and Yang, M.: Precipitation over the Tibetan Plateau during recent decades: a review based on observations and simulations, Int. J. Climatol., 38, 1116-1131, https://doi.org/10.1002/joc.5246, 2018.

Wang, Y., Zhou, B., Qin, D., Wu, J., Gao, R., and Song, L.: Changes in mean and extreme temperature and precipitation over the arid region of northwestern China: Observation and projection, Adv. Atmos. Sci., 34, 289-305, https://doi.org/10.1007/s00376-016-6160-5, 2017.

Wang, Z., Lin, L., Yang, M., and Xu, Y.: The effect of future reduction in aerosol emissions on climate extremes in China, Clim. Dynam., 47, 2885-2899, https://doi.org/10.1007/s00382-016-3003-0, 2016.

Wilks, D.: On “field significance” and the false discovery rate, J. Appl. Meteorol. Clim., 45, 1181-1189, https://doi.org/10.1175/JAM2404.1, 2006.

765 Xiong, L., Yan, L., Du, T., Yan, P., Li, L., and Xu, W.: Impacts of climate change on urban extreme rainfall and drainage infrastructure performance: a case study in Wuhan City, China, Irrig. Drain., 68, 152-164, https://doi.org/10.1002/ird.2316, 2019.

Xu, H., Chen, H., and Wang, H.: Future changes in precipitation extremes across China based on CMIP6 models, Int. J. 770 Climatol., 42, 635-651, https://doi.org/10.1002/joc.7264, 2022a.

Xu, H., Chen, H., and Wang, H.: Detectable human influence on changes in precipitation extremes across China, Earth's Future, 10, e2021EF002409, https://doi.org/10.1029/2021EF002409, 2022b.

775 Xu, K., Xu, B., Ju, J., Wu, C., Dai, H., and Hu, B. X.: Projection and uncertainty of precipitation extremes in the CMIP5 multimodel ensembles over nine major basins in China, Atmos. Res., 226, 122-137, https://doi.org/10.1016/j.atmosres.2019.04.018, 2019.

Yang, X., Zhou, B., Xu, Y., and Han, Z.: CMIP6 evaluation and projection of temperature and precipitation over China, Adv. 780 Atmos. Sci., 38, 817-830, https://doi.org/10.1007/s00376-021-0351-4, 2021.

Yatagai, A., Kamiguchi, K., Arakawa, O., Hamada, A., Yasutomi, N., and Kitoh, A.: APHRODITE: Constructing a long-term daily gridded precipitation dataset for Asia based on a dense network of rain gauges, Bull. Am. Meteorol. Soc., 93, 1401-1415, https://doi.org/10.1175/BAMS-D-11-00122.1, 2012.

785

Ying, X., Bing, Z., Bo-Tao, Z., Si-Yan, D., Li, Y., and Rou-Ke, L.: Projected flood risks in China based on CMIP5, Adv. Clim. Change Res., 5, 57-65, https://doi.org/10.3724/SP.J.1248.2014.057, 2014.

Zhang, W., & Zhou, T. (2020). Increasing impacts from extreme precipitation on population over China with global warming. 790 Science Bulletin, 65(3), 243-252. https://doi.org/10.1016/j.scib.2019.12.002

Zhao, X., Li, H., and Qi, Y.: Are Chinese cities prepared to manage the risks of extreme weather events? Evidence from the 2021.07. 20 Zhengzhou Flood in Henan Province, SSRN Elect J., 4, 3303, http://dx.doi.org/10.2139/ssrn.4043303, 2021.

795 Zhu, J., Huang, G., Wang, X., Cheng, G., and Wu, Y.: High-resolution projections of mean and extreme precipitations over China through PRECIS under RCPs, Clim. Dynam., 50, 4037-4060, https://doi.org/10.1007/s00382-017-3860-1, 2018.